

Proposal for a small-angle X-ray scattering  
instrument at SOLEIL : scientific case and  
brief description

Version 1.3a

# Proposal for a small-angle X-ray scattering instrument at SOLEIL : scientific case and brief technical description

April, 5th, 2002

Spokesperson: Javier Pérez  
LURE, Université Paris-Sud, Bât. 209D  
BP 34  
91898 Orsay Cedex  
Tél & Fax : 01 64 46 80 83  
e-mail: javier.perez@lure.u-psud.fr

Contributors: Franck Artzner<sup>1</sup>, Philippe Barois<sup>2</sup>, Claudie Bourgaux<sup>3</sup>, Patrick Davidson<sup>4</sup>, Olivier Lyon<sup>3</sup>, André Naudon<sup>5</sup>, Pierre Panine<sup>6</sup>, Javier Pérez<sup>3</sup>, Patrice Vachette<sup>3</sup> and Thomas Zemb<sup>7</sup>

- 1 UMR 8612(CNRS)  
92296 Châtenay-Malabry Cedex
- 2 Centre de Recherche Paul Pascal, CNRS  
33600 Pessac
- 3 LURE  
91898 Orsay
- 4 Laboratoire de Physique des Solides  
91405 Orsay
- 5 Laboratoire de Metallurgie Physique, UMR 6630 du CNRS  
86962 FUTUROSCOPE-CHASSENEUIL CEDEX
- 6 ESRF  
38043 Grenoble
- 7 Service de Chimie Moléculaire  
C.E. A. / Saclay  
91191 Gif-sur-Yvette cedex

Technical advisers: Peter Boesecke (ID1 / ID2 at ESRF), Mourad Idir (LURE), Olivier Marcouillé (LURE), François Polack (LURE) and Jean-Paul Simon (D2AM, CRG at ESRF)

Persons having expressed interest in the beam-line design and construction: Claudie Bourgaux as an associate scientist, Olivier Lyon, Pierre Panine and Javier Pérez

Person possibly in search of a permanent position to develop the instrument: Pierre Panine, ESRF Post-doc (ID02)

Present beam-line committee: Franck Artzner, Claudie Bourgaux, Olivier Lyon, Michel Ollivon, Pierre Panine, Javier Pérez, Annette Tardieu and Patrice Vachette

## Outline

<i>Introduction</i> .....	3
<i>Scientific background</i> .....	5
<b>Biophysics</b> .....	5
<b>Material Sciences</b> .....	7
<b>Soft Condensed Matter</b> .....	10
<b>Possible Industrial Applications</b> .....	14
<i>Instrumental considerations</i> .....	15
<b>Context</b> .....	15
<b>Technical aims</b> .....	15
<b>Brief Description</b> .....	16
Source .....	16
Electron beam parameters .....	16
Insertion device .....	16
Pinhole.....	18
Optics .....	18
Mirrors.....	18
Monochromators .....	19
Slits.....	20
Beam position and intensity detectors.....	20
Vacuum and cooling .....	21
Experimental set-up.....	21
Sample environment support.....	21
Detection .....	21
Implantation .....	22
Sample environments .....	23
Support hutch .....	23
In summary : What are the main advantages of this SAXS beamline ? .....	24
<b>Rough estimate of the cost</b> .....	26
Optics .....	26
Infrastructure .....	26
Experience .....	26
<i>Appendix 1</i> .....	27
<i>Support to the project</i> .....	31
<b>Biology</b> .....	31
<b>Soft Condensed Matter</b> .....	32
<b>Metallurgy</b> .....	33
<b>Others</b> .....	34
<i>Bibliographic references</i> .....	35

## Introduction

The present proposal aims at defining a high performance, “easy-to-use” beamline, which would fit with the specific needs of users willing to perform Small Angle X-ray Scattering (SAXS) experiments, no matter their scientific discipline. The SAXS technique has largely developed since the pioneering work of A. Guinier : it was then recognized that “the continuous scattering in the neighborhood of the direct beam is related to the existence of heterogeneities in the matter, these heterogeneities having dimensions of several tens to several hundred times the X-ray wavelength”. Indeed, the scattering at small angles of X-rays (or neutrons) yields incomparable information on the size and morphology of the electronic (nucleonic) heterogeneities, on their size distribution and on their mutual interactions. These measurements are performed on such a large number of particles that reliable mean values can be extracted from them.

The development of Synchrotron Radiation (SR) centers has boosted these types of experiments, mainly through two of the SR characteristics. First, the flux is many orders of magnitude higher than that emitted by classical sources, which allows to study much weaker scatterers samples, or in-situ time dependent phase transitions. Secondly, the SR sources (specially undulators) have very small divergences in both horizontal and vertical directions. Since SAXS experiments give information in the reciprocal space, the larger the scattering particle, the smaller the scattering angle. Therefore, the scale of observable particles depends strongly on the quality of the beam (low divergence, high collimation). One last, but not least quality of SR for such experiments is the energy tunability which allows to adapt the X-ray wavelength to the sample (for example, biological samples require to minimize the absorption because of X-ray damages, whereas metallurgical samples may need to avoid exciting any strong fluorescence). The tunability can also be used to perform labeling experiments: each type of atom contributing (or not contributing) to the scattering can be revealed through the variations of its atomic scattering factor which appear when tuning the X-ray wavelength near its absorption edge (the technique is called ASAXS, for anomalous SAXS).

All these characteristics explain why the concerned fields of research are so numerous, from biology (viruses or macromolecules...), to soft condensed matter (polymers, vesicles...) or material science (aggregates, precipitates..), the studied samples being liquids, gels or solids in transmission, or even in reflection (the technique is called GISAXS , for grazing incidence SAXS and is widely used to study nanomaterials).

Our feeling is that the technical specificities required for an excellent SAXS beamline, in terms of optics and general settings, are basically the same whatever the scientific interest of the user. The slits will be designed and manufactured to minimize the background signal, so as to make full use of the high natural collimation of the beam emitted by the undulator. The beam quality of future undulators on Soleil will be fully exploited to obtain altogether a small and virtually constant beam size whatever the detector position. In particular, the estimated vertical size of the beam (FWHM) should allow to reach  $Q_{\min} = 2.5 \cdot 10^{-4} \text{ \AA}^{-1}$  at 10 m. This resolution of 2.5 micrometers would allow most USAXS (ultra small angle SAXS) experiments to be carried out in the usual pinhole geometry, instead of having to perform Bonze and Hart measurement with an analyser.

Conversely, all the requirements which are specific to a scientific community or to a peculiar experiment should essentially concern the sample environment. This is an essential

aspect of our proposal, namely to supply the user with a variety of possible “up-to-date” sample environments and to make the interchange of sample environments extremely flexible. A final important characteristic of the beamline, as referred to in the general goal, is its easiness of use, especially for a non-specialist user (many of them are expected to arise once the beamline is fully operational). Strong commitment should thus be put to automate wherever possible the operation of the beamline.

Several SR SAXS beamlines exist in France and all of them are overloaded with user requests. ID02 at the ESRF has inspired many of the aspects of the present proposal, especially concerning the detection system. However, in comparison with ID02, we should benefit of an even better quality X-ray beam (essentially lower vertical size and divergence) and of the possibility to explore a range of energies between 5 keV and 15 keV without sacrificing any performance at 12.4 keV, which should be the standard wavelength. Despite the main demand is at fixed wavelength (around 1 Å), the impossibility to perform anomalous experiments would have appeared to us as an error for the future.

Under such considerations, the proposed SAXS beamline will have an unsurpassed flexibility and easiness of use which, with a somewhat lower brilliance compared to the ESRF undulators, will largely overrun its bending magnet sources.

## Scientific background

Mesoscopic (1 nm - 1 $\mu$ m) structures and textures are central to industrial processes estimated to account for half of the industrial activity<sup>1</sup> and are the origin of many problems of basic research dealing with molecular self-organisation at different scales in liquids and solids. Many scientific fields, like molecular biophysics, material sciences and nano materials have a direct interest in the elucidation of the observed mesoscopic organisations and in their thermodynamic and functional modeling.

### Biophysics

Molecular biophysics uses SAXS to study the organization of membranes and of biopolymers like DNA and proteins, the interactions between proteins and/or lipids contributing to rationalize their crystallization and to the solubilization of membrane proteins. Functional biological systems at a higher level of integration are also studied like muscle, molecular motors or cellular organelles like ribosomes [1]. Molecular biophysics also studies the conformation of biological macromolecules [2] (cf insert 2), their conformational modifications associated with catalytic or regulatory properties [3], the formation of complexes with partner molecules (small ligands, proteins, nucleic acids or lipids) often central to their activity [4-7], or even the association of a very large number of molecules leading to supramolecular assemblies like viruses [8], microtubules or other organelles. These studies are presently undergoing a spectacular expansion associated with the development of powerful data analysis software [9-14], with the improvement of the quality of data recorded with synchrotron radiation, particularly at third generation rings; and finally with the increasing availability of high resolution tridimensional structures (protein crystallography, NMR) [15] which constitute a starting point for the analysis of protein conformations in solution, isolated or within a complex. Within the field of molecular biology in which structural genomics comes as a complement to genome sequencing, small-angle X-ray scattering is one component of post-genome structural studies. To compare the three-dimensional structure in the crystal and on solution [16-19], to validate the existence in solution of an oligomer or of a complex characterised in the crystal [20] (cf insert 1), to determine the mode of association of two partners whose complex cannot be crystallised, to characterise the frequently observed rigid body movement of protein domains following ligand binding [4,6,21], to study the (un)folding of a protein following a physico-chemical perturbation (temperature, pressure, denaturing agent) [22-26], to contribute to the optimisation of crystallisation conditions [27], these are but a few of the questions solution scattering can address. All those conformational transitions can be studied at equilibrium (titration) or far from equilibrium by provoking a fast perturbation of the system and following the relaxation towards the new equilibrium state [22,23,26,28]. Finally, it has been shown that low resolution crystallography can provide very useful information on large particles like viruses, whose nucleic acid is only ordered at low resolution [29]. The possibility of collecting such data should be planned at the design stage of the SAXS instrument.

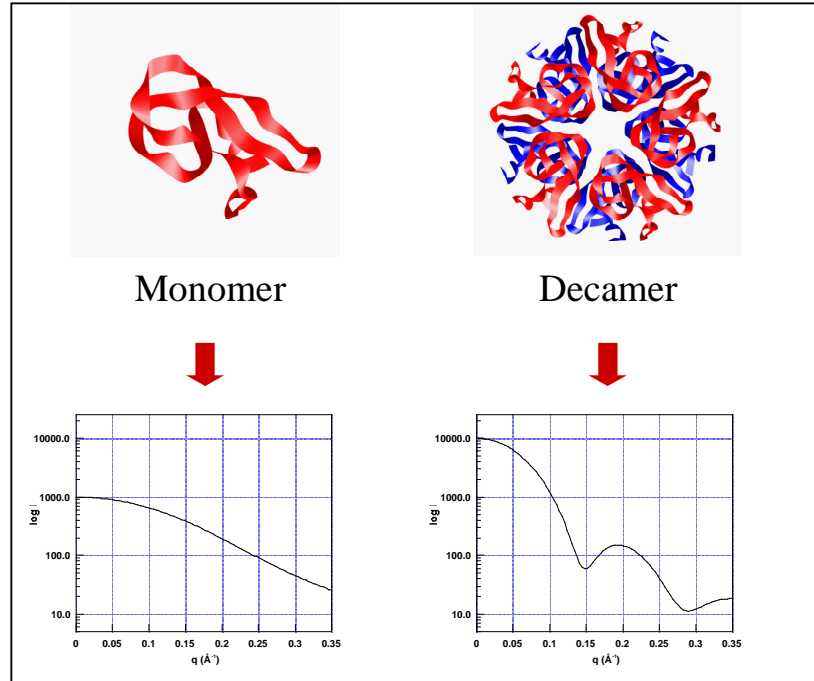
---

<sup>1</sup> see Acad. of Sciences Report "organized molecular systems", report RST RST n°7 july 2000 Tec & Doc editor, Paris

## Insert 1

### BPTI Decamers Observed in Crystals Pre-exist as Stable Species in Solution<sup>#</sup>

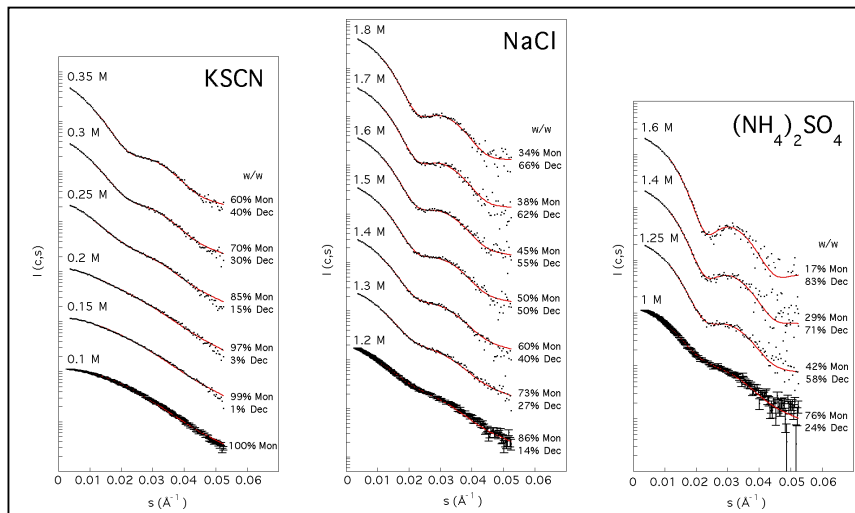
Bovine Pancreatic Trypsin Inhibitor (BPTI) crystallizes at acidic pH in the presence of thiocyanate, chloride and sulfate ions leading to three different polymorphs in P2<sub>1</sub>, P6<sub>4</sub>22 and P6<sub>3</sub>22 space groups. In all these crystal forms, the same decamer is found in the packing (ten BPTI molecules organized through two perpendicular 2-fold and 5-fold axes as a well defined and compact object) in contrast to what is known at basic pH where only monomeric crystal forms are observed. The crystallization process of BPTI under acidic conditions (pH=4.5) was investigated by Small Angle X-ray Scattering (SAXS) measurements on both under- and supersaturated BPTI solutions. Data were interpreted in terms of the formation of discrete oligomers (n=1 to 10).



*Model curves calculated from the BPTI crystallographic coordinates using CRY SOL [Svergun et al. (1995), J. Appl. Cryst. 28, 768-773].*

Calculated scattering curves were obtained using models based on the crystallographic structures and the experimental patterns were analyzed as a linear combination of the model curves using a non-linear curve fitting procedure.

The results, confirmed by gel filtration experiments, unambiguously demonstrate the co-existence of two different BPTI particles in solution: a monomer and a decamer, without any evidence for other intermediates. Moreover, the fraction of decamers was found to increase with increasing salt concentration (i.e. when reaching and crossing the solubility curve). This prompts us to propose that at acidic pH, BPTI crystallizes following a two step process: decamers are first built in under- and super-saturated solutions, upon which crystal



*Experimental curves fitted (in red) by linear combinations of the monomer and decamer model curves. The corresponding weight fractions of each species are given on the r.h.s. of each curve.*

growth proceeds by decamer stacking. Indeed, those BPTI crystals should best be described as "BPTI decamer" crystals.

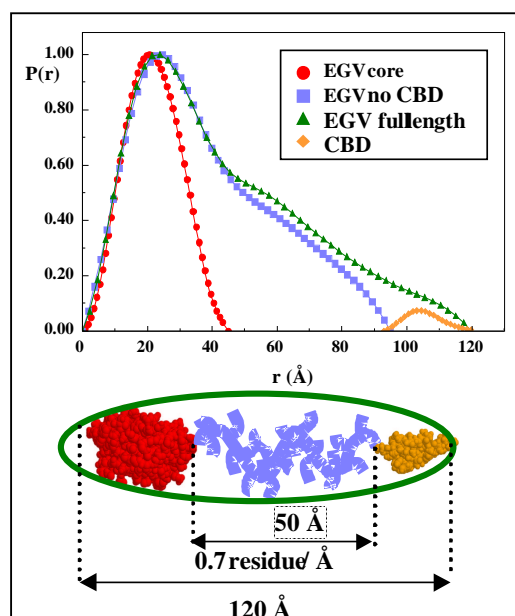
<sup>#</sup> Hamiaux, Pérez, Prangé, Veesler, Riès-Kautt and Vachette (2000). J. Mol. Biol., **297**, 697-712.

## Insert 2

### Solution Structure of Full-length Cellulases Determined by Small Angle X-Ray Scattering

Véronique Receveur, Mirjam Czjzek, Bernard Henrissat, Martin Schülein\*  
 AFMB-CNRS, 31 Chemin Joseph Aiguier, 13402 Marseille cedex 20, France  
 \* Novo Nordisk, Novo Allé, DK-2880 Bagsvaerd, Denmark

While the 3-D structures of a number of isolated catalytic or carbohydrate-binding domain (CBD) of glycoside hydrolases are already available, the global structure of full-length plurimodular enzymes is poorly known. In fact, it has proven so far virtually impossible to crystallize a two-domain cellulase, presumably because of the flexibility and/or heterogeneous glycosylation of the linker peptide separating the domains. Therefore Small Angle X-ray Scattering experiments have been performed on *Humicola insolens* cellulases. Cel45 is a two-domain cellulase with a catalytic domain and a CBD separated by a 36 aa O-glycosylated linker peptide. Full length Cel45 and several of its variants (with no CBD, with modified linkers and the isolated catalytic domain) have been studied. The radius of gyration of the proteins have been measured. The distance distribution function and the maximum dimension inferred from the scattering profiles have given valuable information on the possible conformations of the whole protein and especially of the linker peptide. Our results combined with the available 3-D structures of the isolated domains indicate that the contribution of the linker on the overall size of Cel45 is very important compared to the CBD which has the same number of amino acids. The linker is probably quite extended. Moreover the amino acid composition of the linker seems to govern its flexibility. Finally its glycosylation appears to play a significant role on the possible conformations of the linker peptide. In light of these results, structure-function relationships of full-length cellulases can be discussed.



*Distance distribution function of truncated and full-length EGV and of the isolated domains obtained by small angle scattering experiments from synchrotron radiation.*

## Material Sciences

In material sciences, studies are developing along two main directions: nanoprecipitates in the bulk and thin layers of nanomaterials [30]. In the bulk, the morphology, organization and chemical composition of the nanoprecipitates are to be determined. The chemical composition can be obtained using the so-called "anomalous labelling" [31] (i.e. the variation of the atomic scattering factor as a function of photon energy close to the absorption edge of the investigated element). This labelling method can be applied to a variety of systems like metal alloys, colloids, ferrofluids or polyelectrolyte gels. This kind of study obviously requires a continuously tunable wavelength. On monocrystals, correlations will be determined between the size and shape of the precipitates (studied by small-angle scattering) and the displacement fields [32] (obtained by measuring the Huang scattering around Bragg peaks, cf insert 4). The knowledge of these distortions are crucial for a better understanding of

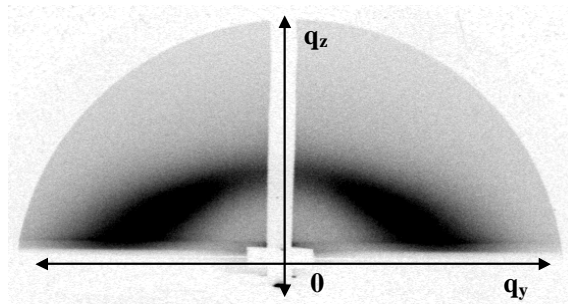
the mechanisms of demixion of real metal alloys which are very different from the isotropic and continuous models usually used.

The research on thin layers of nanomaterials is undergoing an explosive development. These play an increasingly important role in several technological domains like optoelectronics, non linear optics [33] (semi-conductor or metallic nanocrystals in a dielectric matrix), catalysis [34] (Pt or Pd-Pt clusters), magnetic thin [35] or multi layers [36] (Fe and Co clusters in insulating or conductive non-magnetic matrices), nano-electronics, carbon nanotubes, etc. In all cases, the nanoclusters are present in thin layers, supported or buried, and must be studied using grazing incidence techniques (GISAXS, cf insert 3) to obtain information on the size, shape and distribution of these clusters [37-40]. The use of anomalous scattering (AGISAXS) further expands the potential of the method by enabling one to retrieve from the scattering pattern the contribution of a given element (metal clusters in a mesoporous silicon network, nanoclusters included in a rough layer, metals encapsulated in a network of carbon nanotubes).

### Insert 3 Grazing incidence small-angle x-ray scattering (GISAXS)

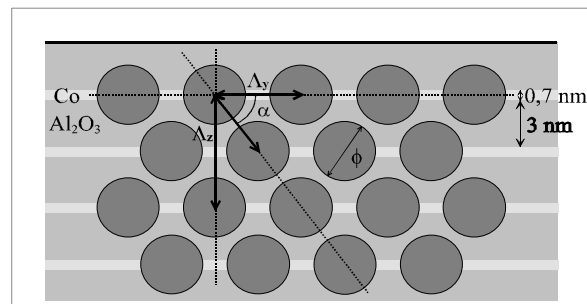
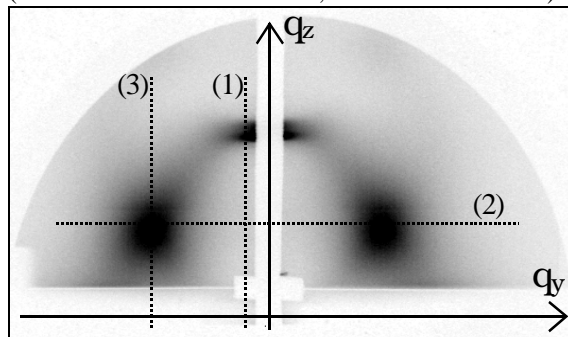
This technique allows one to investigate the morphology of nanoparticles either deposited on a flat surface or buried inside a thin surface layer. It works also very well for a granular multilayer. The two examples hereunder show these possibilities.

#### Nanoparticles buried inside a thin surface layer (UMR 6630 Poitiers)



*Co-deposition of a 1000 Å layer (C 70% - Cu 30%).  
The shape of the copper nanoparticles is anisotropic: They are elongated in the growth direction of the layer.  
 $\Lambda_y = 40 \text{ Å}$  et  $\Phi_y = 26 \text{ Å}$   
 $\Lambda_z = 61 \text{ Å}$  et  $\Phi_z = 52 \text{ Å}$   
Cabioc, Naudon, Jaouen, Thiaudiere and Babonneau (1999).  
Phil. Mag. B, 79, pp 501-516*

#### Nanoparticles in a granular multilayer ( $\text{Al}_2\text{O}_3$ , $30 \text{ Å}$ /Co $7 \text{ Å}$ )<sub>30</sub> (collaboration with F. Petroff, UMR CNRS/Thalès)



*Evidence for a self-organized growth in granular Co/Al<sub>2</sub>O<sub>3</sub> multilayers*

*Left : GISAXS pattern. Right : Scheme of the organization*

*Babonneau, Petroff, Maurice, Vaurès, Naudon (2000). Applied Physics Letters 76, 2892-2894.*

**Insert 4**  
**ASAXS and AWAXS study of a Cu-Ti single crystal**  
 O. Lyon (Iure), J.P. Simon (Itpcm Grenoble) and C. Servant (Imp Orsay)

ASAXS measurements were performed on a  $\text{Cu}_{0.03}\text{Ti}$  single crystal in which  $\text{Cu}_4\text{Ti}$  precipitates were formed by thermal aging: this allowed to determine the size, morphology and composition of the precipitates. The AWAXS appearing around Bragg peaks are due to distortions of the atomic positions of Cu atoms and not to the segregation of Ti atoms. The antisymmetric part of the scattered intensity (i.e.  $I(q)-I(-q)$ ) is simply the projection along the diffraction vector of the Fourier transform of the displacement field. An example is given in the figures below.

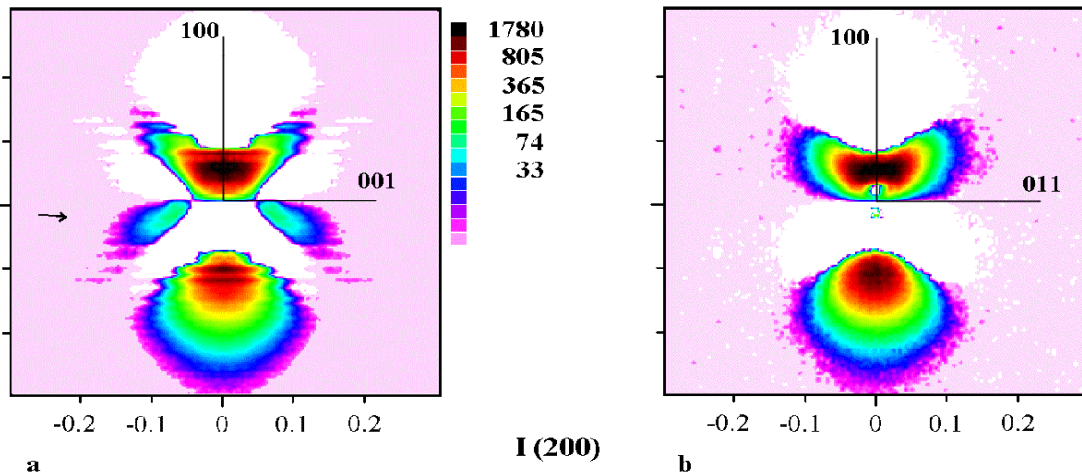


Figure a et b : Around 200 Bragg peak, the antisymmetric part of the scattered intensity were determined for 2 different planes:  $[010]$  in fig. a and  $[0\bar{1}0]$  in fig b. Intensities are expressed in a log scale and only the positive part is represented, the symmetric negative part being left in white. These two images are almost the same, showing that the displacement fields are formed of a region strongly compressed (corresponding to the strong hump in the  $dq>0$  region) . This compression is accommodated by a dilatation which is visible in the  $dq<0$  region.

The displacement field is such that its main contribution is parallel to the  $\langle 100 \rangle$  direction, the pile-up direction of each precipitate family. These displacements (compression plus dilatation) are located in a perturbed region twice as large as the precipitate itself. A dilatation between two precipitates can be interpreted as a repulsion, when a contraction is like an attraction. It comes to saying that two precipitates are repulsive at short distance and attractive at longer one, an effect which may explain why these precipitates have an unusual regular distribution for such a low solute concentration, as is exemplified by the interference ring of the SAXS spectra .

Lyon, Servant and Simon (2000). J. Appl. Cryst , **33**, 928-937

Modern solid-state chemistry is interested in the controlled synthesis of various micro and mesoporous materials [41,42], most notably in its structural and kinetic aspects. The study of heterogeneous catalysis, of great industrial importance, belongs to the same category. In supported catalysis, it is necessary to determine the "smooth or rough" surface state at the nanometer scale in order to understand the kinetics of reagent adsorption. For the inorganic polymerisation aiming at obtaining the most homogeneous mixed oxides, the knowledge of microdomains and heterogeneities, directly accessible by SAXS with hard X-rays, is crucial. This is also true of the chemistry of low temperature sintering process, used to obtain controlled segregation in materials with special optical properties.

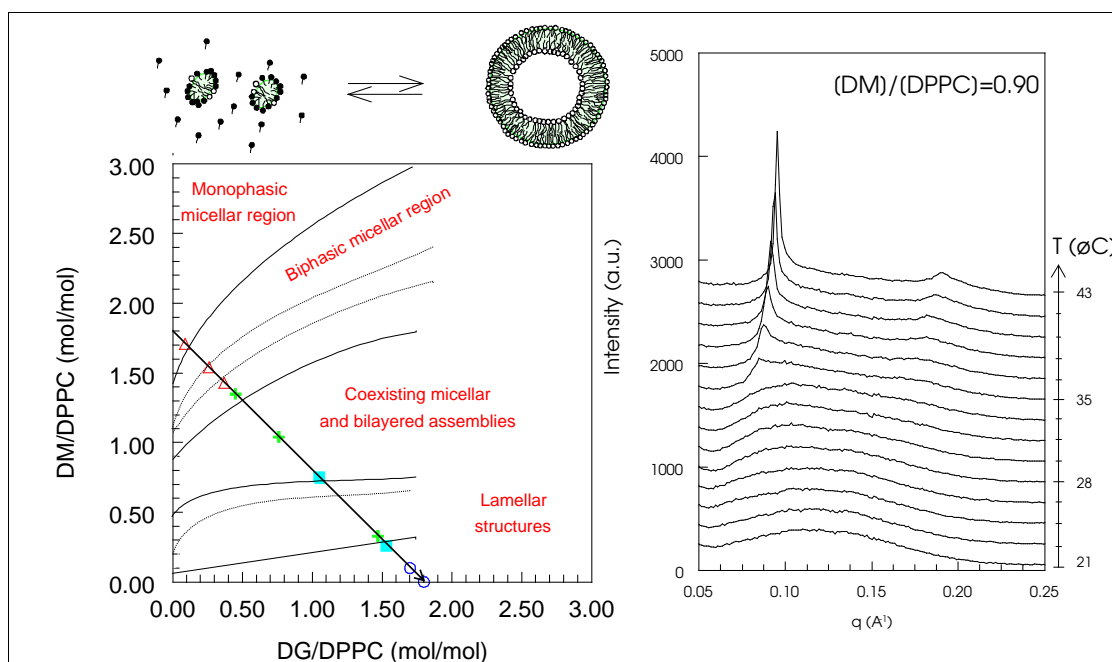
## Soft Condensed Matter

The physico-chemistry of amphiphilic molecules, in particular their solubilisation, their self-assembly, the identification, understanding of the resulting phases (lamellar, hexagonal, cubic, "sponge" phases, ...) and their possible transitions, is one of the traditional fields of use of SAXS methods [43-51] (cf insert 5).

### Insert 5

#### The Micelle-Vesicle Transition (MVT) #

The mixing of lamellar- and micellar- forming long chain molecules leads to the formation of various types of structures, mesophases and aggregates, the interface topology of which ranges from flat to highly curved depending on their proportions. Detergent rich mixtures form highly curved structures, like micelles, while long chain lipid rich ones form flat structures like vesicles. When mixing them in intermediate proportions, a series of mixed aggregates exhibiting intermediate radius of curvatures are formed. The micelle-vesicle transition is the most successful process for the formation of protein-containing vesicles (proteoliposomes) thanks to the difference of solubility in water of lipid and detergent molecules. Then, addition or removal of detergent from mixed lipidic-detergent structures allows the transition. The continuous change of structure and mean radius of curvature during the MVT is comparable to the change in mesophase organisation observed in the temperature-concentration phase diagrams of surfactant water systems. While the overall structure of the mixed aggregates is characterised by scattering and electron microscopy techniques, the local organisation within these aggregates is still unknown as well as all intermediate steps of the MVT. The characterization of the intermediate steps of the MVT can be undertaken by SAXS and WAXS either on equilibrated samples containing various detergent/lipid ratio or by monitoring the MVT. Figure illustrates the induction of the MVT either by enzymatic reaction or by temperature-induced processes. The study of pseudobinary phase diagrams constructed at constant lipid concentration but varying detergent/lipid ratio or temperature has recently shown that several intermediate pseudo-phases could be encountered before the biphasic bilayer-micelle equilibrium took place.



The Micelle-Vesicle Transition process transforms mixed micelles of long chain lipid and short chain surfactant into lipidic vesicles by surfactant depletion of the aggregates (top left). The reverse process known as solubilization corresponds to surfactant addition to solubilize lipidic vesicles. MVT is induced either by an enzymatic reaction (bottom left figure shows the composition path of the lipidic aggregates during the reaction) or by temperature jumps.

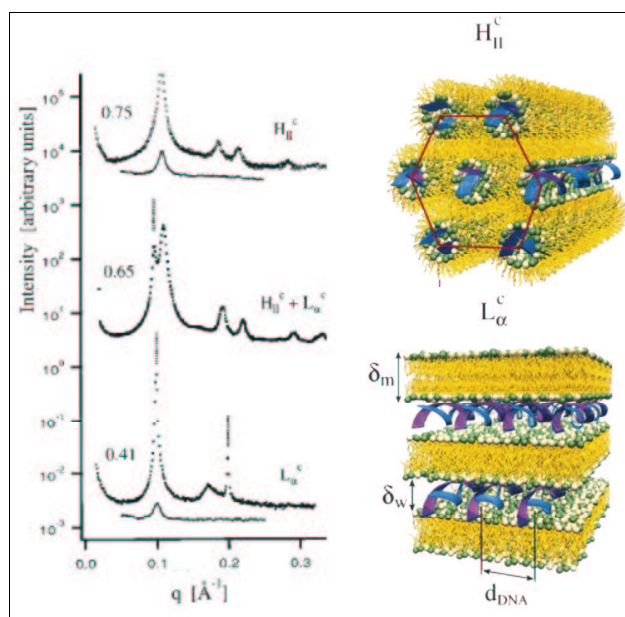
# Ollivon, Paternostre, Lesieur & Grabielle-Madelmont (2000) *Biochim. Biophys. Acta*.

The field of surfactants is moving towards mixed systems with components of various origins: polymeric (latex), mineral (clays) or biological (DNA, proteins or lipids, cf insert 6) [52-61]. In particular, the study of lipids crystallisation in emulsion is developing [62,63]. Surfactants are also used to obtain mesoporous templated structures, with well defined pore sizes and possible hexagonal or cubic symmetry of the porous framework. These structures are obtained through an assembly mechanism where organic species, ionic or non-ionic surfactants or copolymers (template), interact with inorganic precursors (silica,...) of the future inorganic framework [64-66].

### Insert 6

#### Relationship between Lipoplex Structures and Gene Therapy Efficiency

Many human diseases originate from functional deficiency of proteins (genetic diseases,...) or protein concentration aberrations (cancer,...). In gene therapy, cells substitute themselves deficient proteins or regulate their concentrations by expressing genes which are administered to the patient. These genes (DNA) have to be carried into the nuclei of targeted cells. Because of their infection mechanisms, viruses have been successfully tested and are promising vectors. In addition, synthetic DNA carriers such as cationic lipids demonstrated recently their potentiality in non-viral gene therapy. One of the major actual open question is the understanding of transfection mechanism and the improvement of synthetic carrier efficiency. With this aim, a huge progress has been realised by C. Safinya Group at Santa-Barbara (U.S.), which pointed out a relationship between the therapeutically efficiency and the supramolecular structures of DNA/cationic lipids complexes. The complexes with a hexagonal columnar phase  $H_{II}^c$  are more efficient than complexes with lamellar phase. These fundamental conclusions in the field of non-viral gene therapy could not be obtained without the structural characterisation of the complexes by Small Angle X-ray Scattering (SAXS) performed on the high brilliance synchrotron beamline at Stanford.



Synchrotron SAXS patterns (left) of the  $H_{II}^c$  columnar phase (right up) and  $L_{\alpha}^c$  lamellar phase (right down) formed by DNA and cationic lipids. Rädler et al, Science 1997 and Koltover et al, Science 1998.

The new thermotropic mesophases recently discovered often display an organisation on the scale of hundreds of nanometers (twist-grain boundary phases for instance). Furthermore, the field of lyotropic liquid crystals is being enriched with new colloidal objects: biological macromolecules, mineral particles [67-70], etc. (cf insert 7).

SAXS is also widely used to study the organisation of a variety of colloids [71-73] and the structure of gels constituted by 3-D networks of low mass compounds or polymers in a liquid. In the case of physical gels, thermoreversibility can be monitored [74].

The formulation, blending, thermal and mechanical treatments of polymers represent a particularly important industrial stake [75-86]. Fibres can be obtained by controlled crystallisation like Nylon or Kevlar, while spider threads with their exceptional mechanical properties inspire a biomimetic approach. Besides, the field of block copolymers, in solution

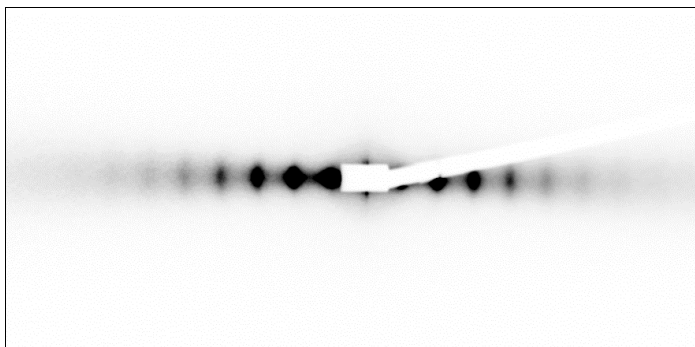
or in the solid state, is rich with ordered microstructures resulting from the low compatibility between the components of these macromolecules [87-89].

### Insert 7

#### A Mineral Liquid-Crystalline Lamellar Phase<sup>#</sup>

Nanometre-scale ordering is well known to appear spontaneously when anisotropic organic moieties form liquid-crystalline phases. This behaviour is also observed for suspensions of anisotropic mineral nanoparticles and its study is currently a challenging and active research area. In this context, we have recently discovered that the layered solid state compound  $\text{H}_3\text{Sb}_3\text{P}_2\text{O}_{14}$  can be exfoliated in water to yield homogeneous, transparent suspensions of extended covalent sheets.

We found that these suspensions form a liquid-crystalline lamellar phase in a wide range of volume fraction  $\phi$ . In this phase, the mineral extended sheets are parallel and regularly stacked. In a SAXS experiment (on ID2 at ESRF), a series of sharp peaks are observed and they can be indexed to the 001 reflections of a lamellar structure. Experiments on very dilute suspensions show that the form factor of the particles is that of 2-dimensional (2-D) planar objects of at least 300 nm diameter. Besides, wide-angle diffraction experiments show the existence of fairly thin diffraction lines which prove that the covalent sheets keep their (2-D) long-range atomic positional order, even at high dilution.



SAXS 2-D scattering pattern of a sample sheared in a Couette cell, in the “tangential” geometry ( $d = 175$  nm).

The lamellar period  $d$  increases as  $\phi$  decreases, i.e. as more water is inserted between the mineral sheets. The lamellar phase actually remains stable down to  $\phi \approx 0.75$  % where the lamellar period reaches 225 nm, to be compared with the covalent sheet thickness of only 1 nm. Thus,  $d$  can be continuously tuned from 1.5 to 225 nm. When  $\phi < 0.75$  %, the suspensions are biphasic with a clear interface between the birefringent lamellar phase and an isotropic phase. This behaviour is indeed that expected for the swelling of a lamellar phase: once the maximum swelling is reached, water molecules can no longer be inserted into the interlamellar space and excess water is expelled. Adding salt affects the swelling behaviour, which strongly suggests that the thermodynamic stability of the liquid crystal is due to electrostatic interactions. This mineral lamellar phase can be very well oriented by mechanical shearing in a Couette cell mounted on the beamline (Figure) or by applying a strong magnetic field as the mineral sheets orient their normal parallel to the magnetic field.

<sup>#</sup> Gabriel, Camerel, Lemaire, Desvaux, Davidson, Batail (2001). *Nature*, **413**, 504.

Beyond the above catalogue, open scientific questions are common to several communities. These communities are usually separated in physics, chemistry, life sciences or science of the universe, not to mention the technological aspect of environmental studies. This dispersion makes exchanges between different communities more difficult, with the exception of some summer schools, some GDRs dedicated to interdisciplinary aspects and some periodic congresses. As an illustration, a few of these questions will be mentioned which are currently investigated in several French groups, and which will still be open when SOLEIL comes into operation:

- Large scale organisation and combination of thermodynamic and kinetic factors in chemical reactions yielding self-assembled structures, the archetype of which is the biomineralisation of calcium carbonate by sea micro organisms: self-assembly is the central problem of the synthesis of mesoporous solids used as catalysts or filters.

- Combination of entropic and electrostatic terms of multicharged systems for which the interaction between charged objects of the same sign can become attractive: this is one of the keys to a better understanding of self-associating polyelectrolytes with complex topology (stars, multi-blocks), of ionomers and other membranes used in fuel cells as well as of numerous biological systems.

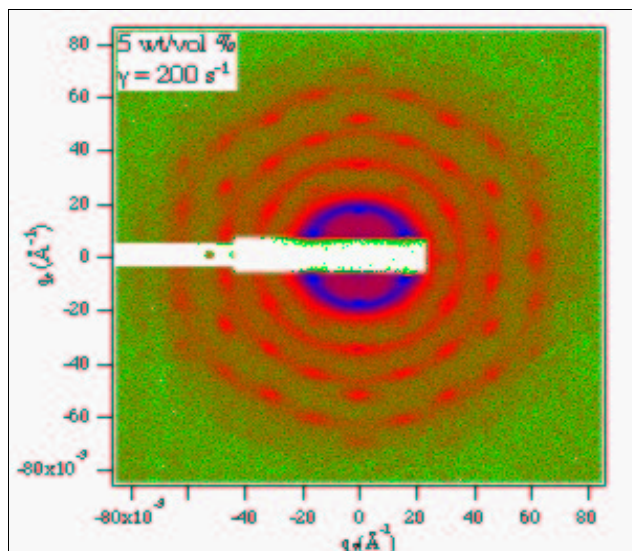
- Smoothness of specially designed long-lasting materials (cements, glasses, vitrocereamics and catalysts) and nanoporosity, the first stage in corrosion, have characteristics driven by mechanisms of dissolution-recondensation. SAXS is perfectly suited for a direct *in situ* characterisation, since classical methods using gas adsorption or thermo-porosimetry are severely perturbing these fragile structures.

- The effects induced by a hydrodynamic shear gradient are diverse (ordering, non linear effects, phase transitions, ...) [90-96] (cf insert 8). Relations between structures and rheological properties are therefore complex. Similarly, dispersion processes (grinding or liquid dispersion) generate poorly characterised stresses within materials. These two classes of problems can be addressed by non-equilibrium experiments (for instance under shear and temperature or concentration gradient). The applications to radiochemistry also belong to this category, since the local accumulation of radicals leads to colloid formation, and therefore to the associated transport. The formation and structure of the colloids formed in a radioactive environment are open questions which could justify the availability of a weakly active sample environment of the kind of light airtight cells used in the biochemistry of radioactive molecules.

### Insert 8

#### Shear induced order in aqueous micellar solutions of amphiphilic polymer diblocks

The immiscibility of the polymeric components of block copolymers accounts for the strong tendency of these materials to self-associate, forming a variety of microstructures. This behavior may be observed either in the melt or in solution in a selective solvent of one of the blocks. Application of an appropriate external field may impart preferential orientation or organization over a macroscopic scale to the microstructure. Aqueous micellar solutions of amphiphilic poly(tert-butylstyrene)-b-poly(Na methacrylate) diblock have been sheared in a Couette cell. SAXS measurements in both the radial and tangential geometries lead to a three-dimensional sampling of the reciprocal space. When the concentration is in the 5-10 w% range, the micelles organize themselves in dense hexagonal layers perpendicular to the velocity gradient. The stacking of planes is random, which is equivalent to a highly twinned fcc structure. The ratio between the intermicellar distance and the interlayer distance is very close to that of a close-packed structure. Experimental data are consistent with a zig-zag motion of adjacent planes upon shear, with jumps between positions extremely close to the registered sites. Shear induced order is restricted to a narrow concentration range just above the critical concentration for gel formation. This domain is thought to correspond to a regime where relative layer translation modes are allowed whereas mutual rotation is hindered. At high shear rates, melting is observed.



Diffraction pattern obtained in the radial configuration at a shear rate of  $200 \text{ s}^{-1}$  (concentration : 5 w% in  $\text{H}_2\text{O}$ )

Leyh, Creutz, Gaspard, Bourgaux and Jerome (1998). *Macromolecules*, **31**, 9258.

- The effect of a magnetic and/or electric field on colloidal suspensions can lead to their crystallisation, thereby generating rich phase diagrams and original rheological behaviours. The use of hydrostatic pressure can also be envisaged.

- The assessment of the hydrophilic-hydrophobic character of interacting biological objects relies on qualitative or very crude bases, such as the relative solubility of an amino-acid in water-octane mixtures. Measurements of interaction potentials between biological objects, finely tuned by the nature of the adsorbed ions, is a common problem to the groups crystallizing proteins, creating artificial viruses like the RNA - polyelectrolytes - peptidic tags or modelling the behaviour of DNA in the presence of histones.

- The organisation of interfaces or of extended defects on the scale of hundreds of nanometers leads to the formation of mesophases like swollen lyotropic cubic phases or TGB phases (twist-grain boundary phases). These structures which reflect subtle equilibria between various interactions can *a priori* be investigated by SAXS.

The combination of SAXS with methods of statistical physics and with a knowledge of interactions (steric, dispersive, electrostatic, entropic) between objects results in a very powerful method of investigation of all these homo and hetero associations.

## Possible Industrial Applications

Many industrial fields have a direct interest in a SAXS beam-line at SOLEIL:

1- Widely used materials, formulation for longer lasting glasses, in bulk or in fibres, and concrete.

2- Metallurgy for the design of alloys, possibly supersaturated (e.g. mechano-chemically produced nanomaterials).

3- Formulation of solid polymers, for all problems associated with the use of linking or compatibilising additives.

4- Solubilisation in emulsions, micro-emulsions and clathrate-like solid microstructures studied in oil industry as applied to the transport of hydrophobic raw materials.

5- The cosmetic industry must justify, for all officially accepted formulations, the existence and preservation of microstructures in gels and creams compatible with perfumes and active components in the container as well as in the conditions of application onto skin and hair. This makes use of micro-beam SAXS.

6- The pharmaceutical industry for drug vectorisation; vaccine diffusion, redispersion of solid tablets, solubilisation in physiological conditions without precipitation, monitoring of parenteral solutions.

7- Food industry: formulation for the distribution of food, from thickening agents to powder dispersion.

8- Mining industry: flotation of ores based on the selective adsorption of surfactants.

9- Biotechnology: e.g. the biomimetic synthesis of structured phosphates, carbonates and mimics of mother-of-pearl.

## Instrumental considerations

### Context

French needs in SAXS are such that two experimental stations are currently dedicated at LURE (D22, D24). Partly or totally dedicated SAXS beamlines exist at ESRF (ID01, ID02, D2AM, BM26), but they cannot cover all the European needs. Our project has tried to capture the best advantages of ID02 and ID01, offering the user a robust beam-line, flexible in terms of sample environments, and tunable in terms of wavelength. We also expect to obtain a smaller natural beam-size at the detector position than on ID02, thus offering a lower minimum value of the scattering vector  $Q$ . Moreover, since the flux delivered by the insertion devices of SOLEIL in the hard X-ray range is smaller by more than one order of magnitude than at the ESRF, for those experiments essentially needing very high flux, we propose an alternative large band-pass monochromator which should deliver a flux comparable (if not higher) than that of ID02.

Several small-angle neutron scattering instruments are available at both the ILL and the LLB, which can provide valuable complementary information to SAXS. For example, anomalous scattering in X-ray experiments and isotopic substitution in neutron experiments may be used as complementary contrast variation techniques : selective deuteration helps in studying the chain of a polyelectrolyte by neutron scattering while X-ray scattering is used to investigate the distribution of the heavier counterions. Moreover, very low  $Q$ -values are more easily obtained with long wavelength neutrons. But on the other hand, neutron flux is much lower than that of a synchrotron source, and the  $Q$ -resolution is much less accurate.

### Technical aims

The applications presented above require an X-ray beam of great optical quality (very low divergence), very intense and tunable in energy (anomalous effect, elimination of a fluorescence, search for a selective information deep into the material thanks to the variation of the penetration length with the photon wavelength). A high beam intensity is a primary requirement for studies of weakly scattering samples, like nanometer thick layers, and for time-resolved monitoring of *in situ* transformations. It is also important to note that the understanding of many phenomena can only be made quantitative if absolute scale measurements can easily be performed. These studies do not make use of two important characteristics of S.R., namely polarisation and coherence. This latter property has started to be used to investigate thermodynamic fluctuations with the advantage over visible light to allow the study of opaque materials and to study much shorter correlation lengths. A SAXS instrument built for the next 30 years should preserve the possibility to use these characteristics.

The instrumental requirements can be summarised as follows:

1- a reliable, rugged and high flux beamline mostly operating at a fixed wavelength and giving access to a very large range of momentum transfer  $q$  ( $q=4\pi \sin(\theta)/\lambda$ ) :

- $q_{\min} \approx 5.10^{-4} \text{ \AA}^{-1}$  ( $d \approx 1.2$  micrometer) on the SAXS detector (for an entirely evacuated beam path).
- SAXS detector diameter  $\geq 20$  cm, pixel size  $\leq 100 \mu\text{m}$ ,

- sample - detector distance  $D_{\min} \approx 0.25$  m,  $D_{\max} \approx 10$  m
  - $q_{\max} \approx 2 \text{ \AA}^{-1}$  on the WAXS detector positioned on a rail with a possible overlap of the two SAXS/WAXS  $q$ -ranges for normalisation
- 2- a minimised scattering background and a stable calibration.
  - 3- a large choice of sample environments fully dedicated to the beamline, available to all users and rapidly and easily interchangeable.
  - 4- wavelength tunability between 5 keV and 15 keV.
  - 5- easy and user-friendly operation of the beamline, providing a relative autonomy of users with respect to the local contact.

These criteria correspond to the performances expected from a SAXS/WAXS beamline mostly operating at a fixed wavelength (around 12 keV at 2.75 GeV) and for a shorter part of the time at variable wavelength between 5 keV and 15 keV.

## Brief Description

### Source

#### *Electron beam parameters*

Table 1 recalls the principal beam characteristics on the short and medium sections. In principle, the horizontal electron beam characteristics on a medium section ( $\sigma=180 \mu\text{m}$ ,  $\sigma'=30 \mu\text{rad}$ ) are better suited for the SAXS beamline project. Indeed, due to the respective source beam sizes, the magnification  $G$  has to be twice as small in the short section case than in the medium section to get the same (small) natural beam size, for a given position of the experimental hutch. Therefore, the focusing element (mirror, in our case) would have to be longer and inserted further from the source in the short section case, thereby generating extra-costs and manufacturing difficulties. However, one should keep in mind that, if necessary, the beam size can also be reduced using slits.

	<b>beam parameters</b>			
<b>straight section</b>	<b>size<sub>x</sub> (FWHM)</b>	<b>size<sub>z</sub> (FWHM)</b>	<b>divergence<sub>x</sub> (FWHM)</b>	<b>divergence<sub>z</sub> (FWHM)</b>
<b>short (1.8 m)</b>	<b>912 <math>\mu\text{m}</math></b>	<b>19 <math>\mu\text{m}</math></b>	<b>33 <math>\mu\text{rad}</math></b>	<b>11 <math>\mu\text{rad}</math></b>
<b>medium</b>	<b>425 <math>\mu\text{m}</math></b>	<b>19 <math>\mu\text{m}</math></b>	<b>71 <math>\mu\text{rad}</math></b>	<b>11 <math>\mu\text{rad}</math></b>
<b>ID02 (ESRF)</b>	<b>1030 <math>\mu\text{m}</math></b>	<b>210 <math>\mu\text{m}</math></b>	<b>43 <math>\mu\text{rad}</math></b>	<b>27 <math>\mu\text{rad}</math></b>
	<b>X</b>		<b>Z</b>	
<b>Emittance</b>	<b>3.63 nm rad</b>		<b>0.036 nm rad</b>	
<b>Energy</b>	<b>2.75 GeV</b>		<b>radius</b>	<b>5.817 m</b>

**Table 1: Soleil beam parameters**

#### *Insertion device*

The undulator U20 with a minimum gap of 5 mm ( $K=1.85$ ) would be perfectly suited to work at 12.4 keV and to perform measurements between 5 and 15 keV as well, including anomalous experiments. On the one hand, the small period (20 mm) allows high flux and brilliance at 12.4 keV. On the other hand, with a mini-gap of 5 mm, the variation of brilliance and flux with wavelength is smooth enough within a given harmonic and exhibits

discontinuities from one harmonic to the next which do not exceed a factor of 3 in flux or brilliance, which is crucial for the anomalous experiments. However, U20 cannot be inserted in a medium section, because of a potential damaging effect on the electron beam lifetime, and the 5 mm gap is no more guaranteed by Soleil, even in a short section.

The undulator U26 is less effective than U20 at 12.4 keV if inserted in a short section. Not only its resulting theoretical brilliance is slightly smaller at this energy, but the corresponding harmonic order is much higher (15 instead of 7 for U20), which decreases much more the actual brilliance. However, the performances of a double U26 inserted in a medium section become comparable to those of U20 in a short section (see figure 1). The effect of using a higher harmonic order at 12.4 keV (this time : 11 instead of 7 for U20) leads to an actual brilliance more than half that of U20 in a short section (O. Marcouillé, private communication), while the smoothness of the brilliance variation with energy is improved in the case of double U26.

Thus, a double U26 on a medium section would be one possible choice, which would favour a smaller horizontal natural beam size at the detector position and a very smooth variation of the intensity vs the wavelength. Provided it can be closed to less than 6 mm, U20 on a short section would constitute a second possible choice, which would favour a higher flux at 12.4 keV at the cost of a larger horizontal natural beam size at the detector position. In any case, it is essential that the undulator gap can be modified from the experimental hutch in an easy way so that it can be performed by the local contact and the external users (after some training).

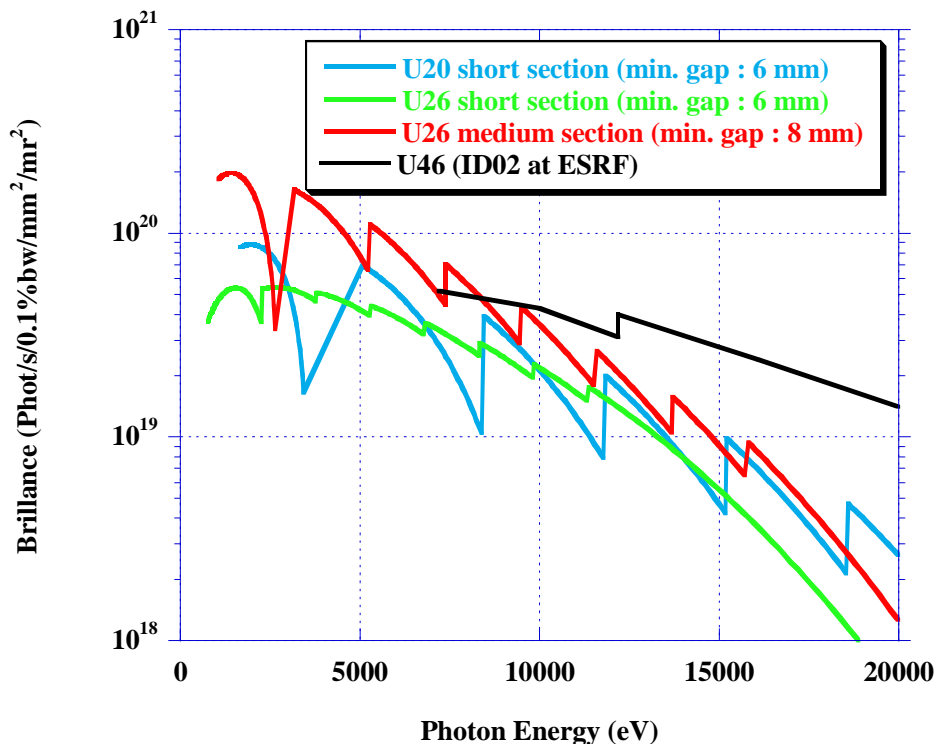


Figure 1 Theoretical brilliance curves of U20 and U26 (O. Marcouillé, LURE). These curves do not take into account the “harmonics effect”. The actual brilliance is all the more smaller than the displayed value as the harmonics number is high. Thus, at 12.4 keV, the actual brilliance of U26 on a medium section is slightly smaller than that of U20 on a short section, despite what is shown. The brilliance of U46 at ESRF is also shown, for the sake of comparison.

### ***Pinhole***

For chronological reasons, the following heat-load calculations have been made considering the U20 undulator on a short section. We are confident that the conclusions would be qualitatively the same for a double U26 on a medium section.

The total power arising from U20 is expected to amount to about 4300 W when the gap is set at 5mm ( $K=1.85$ ). Used as it is, the beam would then produce an enormous amount of heat on the first optical elements, with which it would be impossible to cope. Instead, it is possible to make use of the angular dispersion of the incident beam at a given photon energy (and harmonics) to stop more than 90 % of the total power before the first optical element, virtually without sacrificing the intensity at the working wavelength. Indeed, the simulation of the photon flux angular distribution in the configuration  $K=1.5$  shows that the useful part of the beam, corresponding to the optimised wavelength, is restricted to an area of  $2400 \times 800 \mu\text{m}^2$  around the beam axis at 15 meters from the source (full width at 2% of the intensity Gaussian shape,  $\text{FWHM} = 1000 \times 340 \mu\text{m}^2$ ). This area remains the same whatever the considered harmonics and should only slightly depend on the gap value (area reduced by about 15% for  $K=1.0$  and increased by about 15% for  $K=1.85$ ). Therefore, a cooled pinhole with a variable size, inserted before the first optical element, should absorb the major part of the heat load and deliver a beam of roughly calibrated size.

### **Optics**

The objective of the optical set-up is to deliver a monochromatic beam at a fixed position, the energy of which should be easily adjustable between 5 keV ( $\lambda = 2.48 \text{ \AA}$ ) and 15 keV ( $\lambda = 0.827 \text{ \AA}$ ). It is compulsory that the beam divergence at the detector position should be low, in order not to refocus the beam each time the detector distance is changed (the detector is expected to be displaced over a 10 m range). The beam size should also be small to allow the best possible  $Q_{\text{min}}$  (about  $400 \mu\text{m}$  FWHM in the horizontal plane and less than  $40 \mu\text{m}$  in the vertical plane would be acceptable values). The compromise between size and divergence of the beam at the detector position will have to be carefully chosen (see above, *Electron beam parameters*). The respective positions of the optical devices presented below represent only one possible solution.

The proposed optics essentially consists of a couple of mirrors and a two-crystal monochromator. The principal concept is to separate monochromatisation from focusing to facilitate wavelength tuning. In particular, the monochromator should be composed of plane crystals to avoid any influence of crystal bending during wavelength selection. The set of mirrors is then expected to eliminate high energy photons by absorption and to allow for beam focusing as well.

### ***Mirrors***

The two mirrors (probably Si crystals) are perpendicular to each other in the Kirk-Patrick Baez (KB) configuration. Both mirrors are longitudinally bent to allow focusing in the vertical and horizontal planes, respectively. A sagittal mirror was first planned for horizontal focusing, but the KB configuration was finally preferred, sagittal mirrors being difficult devices to build and to operate. One of the two mirrors will be the first optical device, in order to limit the heat load on the monochromator. The second mirror can be alternatively inserted before or after the monochromator. In the latter case, it does not have to be cooled, which may represent a significant advantage in terms of cost and handling.

In the present state of the project, the second mirror would be inserted after the monochromator. The first mirror would be the vertical focusing mirror, necessarily shorter and therefore easier to cool.

Beside focusing, the mirrors act as low-pass filters, absorbing the high-energy photons which would otherwise be diffracted by the monochromator (as harmonics of the selected wavelength) (see *monochromator*). Unwanted energies range from 15 keV (working energy = 5 keV) to 45 keV (working energy = 15 keV). The set of mirrors has also to deliver the beam at a fixed position in order to minimise the movements of the crystals in the monochromator. To achieve this twofold goal, the angle of incidence on both mirrors is kept fixed, with one of the two mirrors (probably the second one) coated with two different, adequately chosen coatings, in two longitudinal stripes, corresponding to two different cut-off energies for the same angle of incidence. In this way, changing the cut-off energy only requires a lateral translation of this mirror within its own plane, with no movement of the other mirror, thus keeping the beam trajectory unchanged. As the reflectivity curves usually exhibit a long tail on their high energy side, the low cut-off energy should be chosen below 10 keV, so as to virtually eliminate any flux at 15 keV. This could be achieved by a Si surface with an incident angle above 3.3 mrad. The second surface could then consist of a Mo or Pd coating, for which the cut-off energy would then be around 19 keV (see figure 2). The other mirror should of course be coated with the material of high cut-off energy.

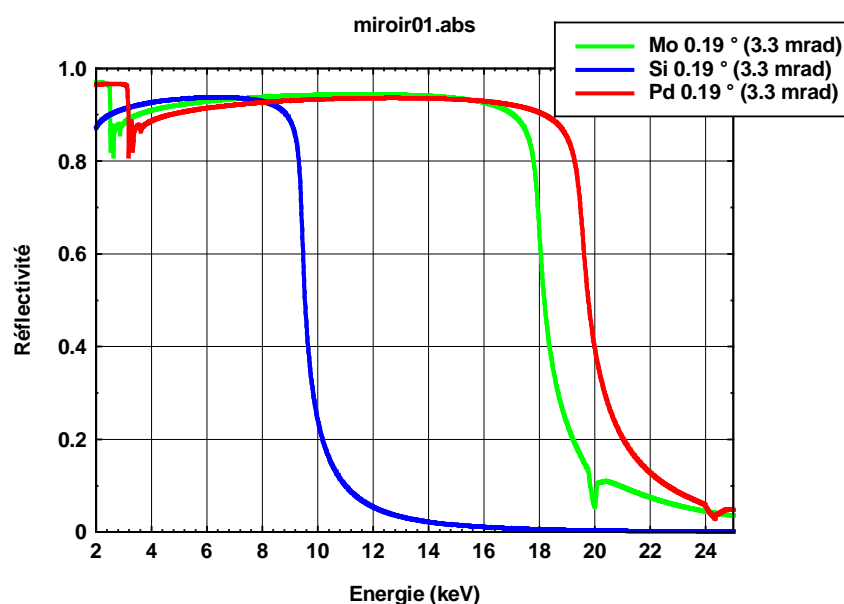


Figure 2 Theoretical reflectivity curves at a fixed incidence angle for three different coatings (from Mourad Idir, LURE)

### *Monochromators*

The high resolution monochromator consists of two parallel Si crystals, which deviate the beam trajectory in the vertical plane. The monochromator having no focusing function, Ge crystals could be alternatively used at energies below 11 keV, if needed. The crystals are inserted in a motorised chamber with a unique horizontal rotation axis, perpendicular to the beam trajectory. A translation motor can move the chamber to bring the rotation axis in coincidence with the beam position at the surface of the first crystal. The wavelength selection is made possible by rotating the chamber around the surface of the first crystal. The

second crystal has then to be translated to keep the beam at a fixed position at the monochromator exit. The precise orientation of the second crystal can be adjusted using two rotations controlled by piezoelectric elements.

An optional, broad band-pass monochromator, providing a higher flux, will be developed once the crystal monochromator is operational. It will make use of two separate multilayer elements set up so as to deliver the monochromatic beam at the same position as the crystal monochromator [97]. The multilayer monochromator is intended to operate at a single wavelength around 12.4 keV. As the incidence angle on the multilayers should be about ten times lower than the incidence angle on the Si crystals for the same wavelength, the distance between the two multilayers along the beam should be around ten times longer than that between the Si crystals. Thus, it is proposed that the two multilayers be housed in separate vessels positioned at an equal distance on each side of the crystal monochromator. When needed, the first multilayer should be vertically translated in order to intercept the beam coming from the first mirror. The reflected monochromatic beam would then pass between the two crystals of the high resolution monochromator before being redirected by the second multilayer to the fixed exit position. With this geometry, the change of operating mode only involves the vertical motion of the first multilayer. Most importantly, the crystal monochromator remains properly set up and ready for use.

### ***Slits***

Slits are crucial components of a SAXS set-up to eliminate the parasitic radiation close to the direct beam and, if required, to reduce the size of the beam cross-section (collimating slits). They must be carefully manufactured (cylindrical shape, with the smallest attainable rugosity, made of Mo or Ta). Three sets of slits are planned. The first set,  $S_0$ , is placed just upstream of the monochromator to eliminate the background intensity produced by the first mirror fluorescence and to redefine the beam size, if required. The second set of slits,  $S_1$ , is inserted downstream from the last optical device (monochromator or second mirror). The third set of slits,  $S_2$ , is positioned in the experimental hutch, just in front of the sample to minimise the background produced by  $S_1$ . The distance between  $S_1$  and  $S_2$  has to be large (several meters). The recent development at the ESRF of extremely high quality slits and their associated mechanics makes it possible to reduce the beam size down to some ten(s) of micrometers (at the expense of intensity, of course).

### ***Beam position and intensity detectors***

The automation of the alignment protocol requires the availability of beam position detectors downstream from each optical element.

Two removable position detectors for "white" beam (a couple of tungstene wires, which emit electrons when hit by the beam) will be positioned along the beam path. The first one should be placed before the first mirror to determine the beam position at the exit of the undulator, the second one after the first mirror to adjust its orientation.

Three removable fluorescent screens will be used to detect the monochromatic beam position. The first one will be inserted just before the second mirror to adjust the monochromator orientation, the second one at the end of the optical hutch to be sure that the beam correctly exits the second mirror, and the third one just before the  $S_2$  slits in the experimental hutch to refine the beam position by finely acting on the different optical devices.

To facilitate all settings, the motors controlling the optical element adjustments should be servo-controlled by the information given by the position detectors. Contacts have been

taken with researchers in robotics from the University of Jussieu (Paris) to take care of this important aspect of the project.

The incident intensity should be measured just before the  $S_2$  slits with a pin diode. A filter changer followed by a second pin diode can also be placed between the first pin diode and the  $S_2$  slits to calibrate the energy or to attenuate the monochromatic beam.

### ***Vacuum and cooling***

The optical devices receiving “white beam” should be in ultra-high vacuum and probably nitrogen cooled (heat load calculations are being made). Therefore, a beryllium window should be inserted after the monochromator to separate the ultra-high vacuum section from the following secondary vacuum section, which is in direct connexion with the experimental set-up.

### **Experimental set-up**

The experimental set-up is expected to allow for a fast replacement of the sample environment, together with a fast, reproducible and automated change of detectors position.

### ***Sample environment support***

Sample environments are expected to be diverse and numerous and might be changed several times a week. It is therefore crucial to define a practical protocol which makes these changes as fast as possible. A vertically motorised table of  $1 \times 1 \text{ m}^2$  is positioned between the support of slits  $S_2$  and the front of the detector tube (see *Detection*). On top of this table, a horizontally motorised (X-Y) translation table supports the various sample environments, which are screwed onto it. A second copy of this (X-Y) translation table is used outside the experimental hutch to prepare the positioning of the next sample environment. This second copy is coupled to a laser device which mimics the beam trajectory in order to roughly pre-align the sample environment. To change the sample environment, the whole system ((X-Y) translation table + fixed sample environment) is moved onto the beamline using an elevator on wheels. The final adjustments can be made afterwards, without having wasted beam-time to mount the sample environment.

### ***Detection***

Two bidimensional detectors are planned to be usable at the same time, a high performance SAXS detector, and a WAXS detector, which could be a simpler CCD camera. The SAXS detector characteristics must include :

- small pixel size (at least below 100 micrometers)
- diameter above 20 cm
- actual capacity to measure on a single image a range of intensities differing by 4 orders of magnitude (high dynamics and narrow point-spread function)
- fast reading-time (below 50 ms, if possible)

The SAXS detector presently used on ID02 at ESRF (Thomson intensifier lens coupled to the ESRF developed FRELON CCD camera) seems a good starting-point, despite some problems limit the actual reading dynamics to between 2 and 3 orders of magnitude.

Both SAXS and WAXS detectors should be placed in a large chamber under primary (or secondary) vacuum, and their motions should be motorised to allow access to a large Q-range detection. The detectors chamber is essentially a cylindrical 1.5 m diameter tube of around 11 m long, with a vertical extension at its closer-to-sample end to accommodate the WAXS detector.

The SAXS detector should be installed on a motorised truck (cf ID2 at ESRF) which can be translated along the beam direction to rapidly change the sample-to-detector distance from 0.25 m to *approx.* 10 m. A downward vertical translation of the detector within the tube should also be necessary to bring the detector off-center and thus intercept a larger angular range. This downward position is also necessary to provide the overlapping between the Q-ranges intercepted by the SAXS and WAXS detectors, which is required for mutual calibration of detectors.

The WAXS detector should be placed within the vertical extension of the tube, above the SAXS detector trajectory and on a vertical axis about 50 cm from the sample. It could be centred about the desired average scattering angle using a vertical translation table and it could be oriented around a horizontal rotation axis to bring its detection surface perpendicular to the sample direction.

### Implantation

One satisfactory compromise between horizontal beam size and divergence at the detector position is found with the horizontally focusing mirror at 22 m from the source, the focusing point at 38 m and the detector moving between 33 m and 43 m (see figure 3 and calculations in appendix 1). The distance between slits F1 and F2, about 9 m, would then be sufficient to minimise the background.

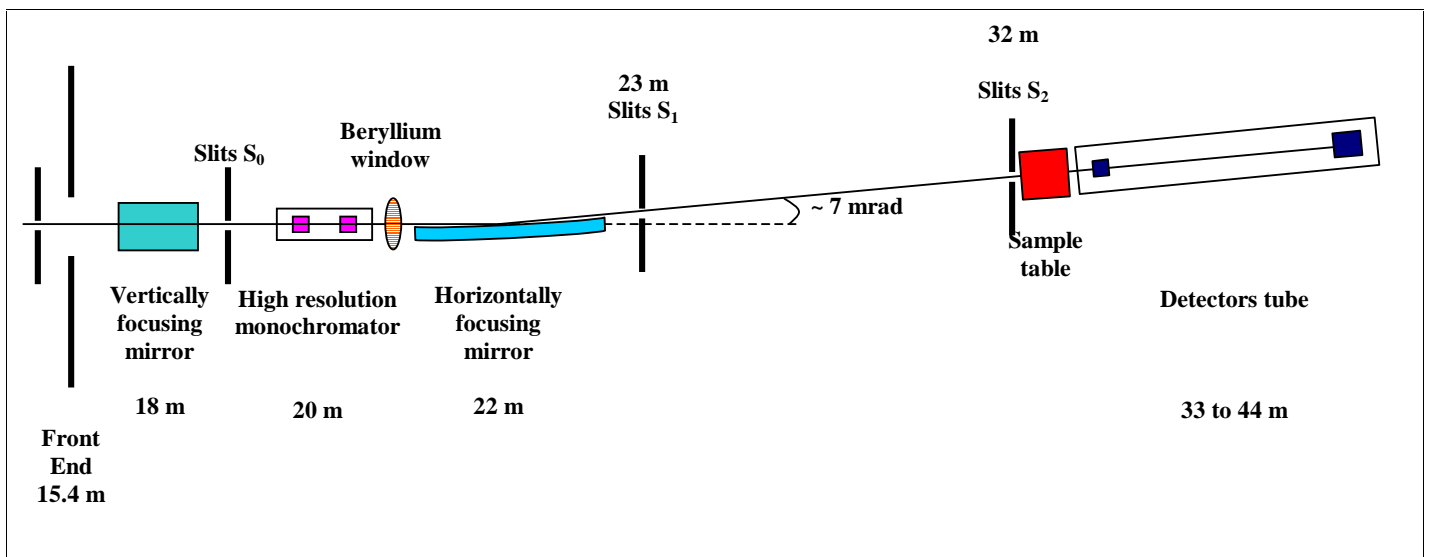


Figure 3 One possible configuration of the SAXS beam-line using the medium section source parameters (seen from above)

With the medium section source parameters, the horizontal natural beam size would be rather small along the whole detector course, about 500  $\mu\text{m}$  (FWHM) at the detector extreme positions and 400  $\mu\text{m}$  for the detector at 5 m (values estimated with a mirror slope error of 1.5  $\mu\text{rad}$  : see appendix 1). The vertical natural beam size would be around 130  $\mu\text{m}$  for the detector position at 5 m and around 155  $\mu\text{m}$  at the detector extreme positions.

**In these conditions, if we consider a beam-stop size 5 times larger than the beam size (FWHM) and a 20 cm diameter detector, the ratio between  $Q_{\max}$  and  $Q_{\min}$  in a single image would be about 80 in the horizontal direction (it is about 40 on ID2 without resizing the beam with slits) and 250 in the vertical direction (it is about 80 on ID2 without resizing the beam with slits).**

The optics hutch should occupy the first 8 to 9 meters after the front end, and be wide enough to provide an easy access to the various optical elements. The experimental hutch should be relatively long (about 15 m) and about 4 m wide. The space situated between the optics hutch and the experimental hutch is not yet precisely defined, but is expected to be several meters long (distance between F1 and F2). This space could be appropriate for a future second experimental hutch devoted to diffraction and diffusion microfocus experiments [98,99] (a removable focusing device after the monochromator could be used to strongly focus the beam at a short distance after the optics hutch). For the time being, it could be advantageously used as a discussion & computing room. A possible general implantation is proposed in figure 4 at the end of the present proposal.

### **Sample environments**

The flexibility and variability of sample environments has to be one of the fundamental characteristics of the beam-line, in order to answer the great variety of the requirements of the scientific communities. As previously described, the frequent changes of sample environments, which are either locally proposed to the users or brought by them, make a pre-alignment hutch necessary. The experiments are expected to be carried out either under vacuum or in air, depending on the set-up.

Here is a first list of sample environments which should be made locally available to the users, with no special order of priority and no claim to exhaustivity:

- A- thermostated changer for vacuum tight cells
- B- thermostated set-up under vacuum for liquid samples with sample circulation
- C- thermostated stretching device
- D- calorimeter (coupling DSC with SAXS/WAXS)
- E- Couette cell (coupling rheology with SAXS/WAXS)
- F- thermostated stopped-flow mixer
- G- a one axis goniometer with cold nitrogen flow for low resolution protein crystallography
- H- High-pressure cell
- I- GISAXS set-up : this particular set-up has been developed by O. Lyon at LURE and could be directly transposable to SOLEIL virtually without further costs.

### **Support hutch**

A support hutch, dedicated both to the preparation of various kinds of samples and to the prealignment of sample environments, is required. This support hutch is not expected to replace the more specialised biochemistry and chemistry laboratories, which should be as close as possible from the SAXS beam-line. However, some minimal equipment is required for sample preparation:

- a small cold room
- a laminar flux hood
- a refrigerator
- a high precision balance

- an oven
- a microscope, etc.

Several fluids should also be available for general purposes:

- compressed air
- nitrogen gas
- demineralised water

**In summary : What are the main advantages of this SAXS beamline ?**

The beam quality of undulators on Soleil is fully exploited to obtain altogether a small and virtually constant beam size at the detector position. In particular, the estimated vertical size of the beam (FWHM) is expected to vary between 130 and 155  $\mu\text{m}$  throughout the detector course, which corresponds, in principle, to  $Q_{\text{min}} = 2.5 \cdot 10^{-4} \text{ \AA}^{-1}$  at 10 m, considering a beam-stop vertical width of 0.8 mm. If reached, this resolution of 2.5 micrometers would allow most USAXS experiments to be carried out in the usual pinhole geometry.

The setting-up will be fully automated with the extensive use of beam position monitors throughout the beam path. An expert system will be implemented, first to permanently survey the whole state of the beam-line and react in case of any problem, secondly to help any user to rapidly and confidently modify experimental parameters (wavelength, beam size, detector position, ...).

Multiple experimental environments will be available and will be pre-aligned in a separate hutch before being transferred onto the beam-line. This will altogether save beam-time and give users more time to prepare their experiment.

The slits will be designed and manufactured to minimize the background signal, so as to make full use of the high natural collimation of the beam emitted by the undulator and reach a resolution better than 1 micrometer virtually without reducing the natural beam-size.

Simultaneous SAXS and WAXS measurements will be proposed as a standard.

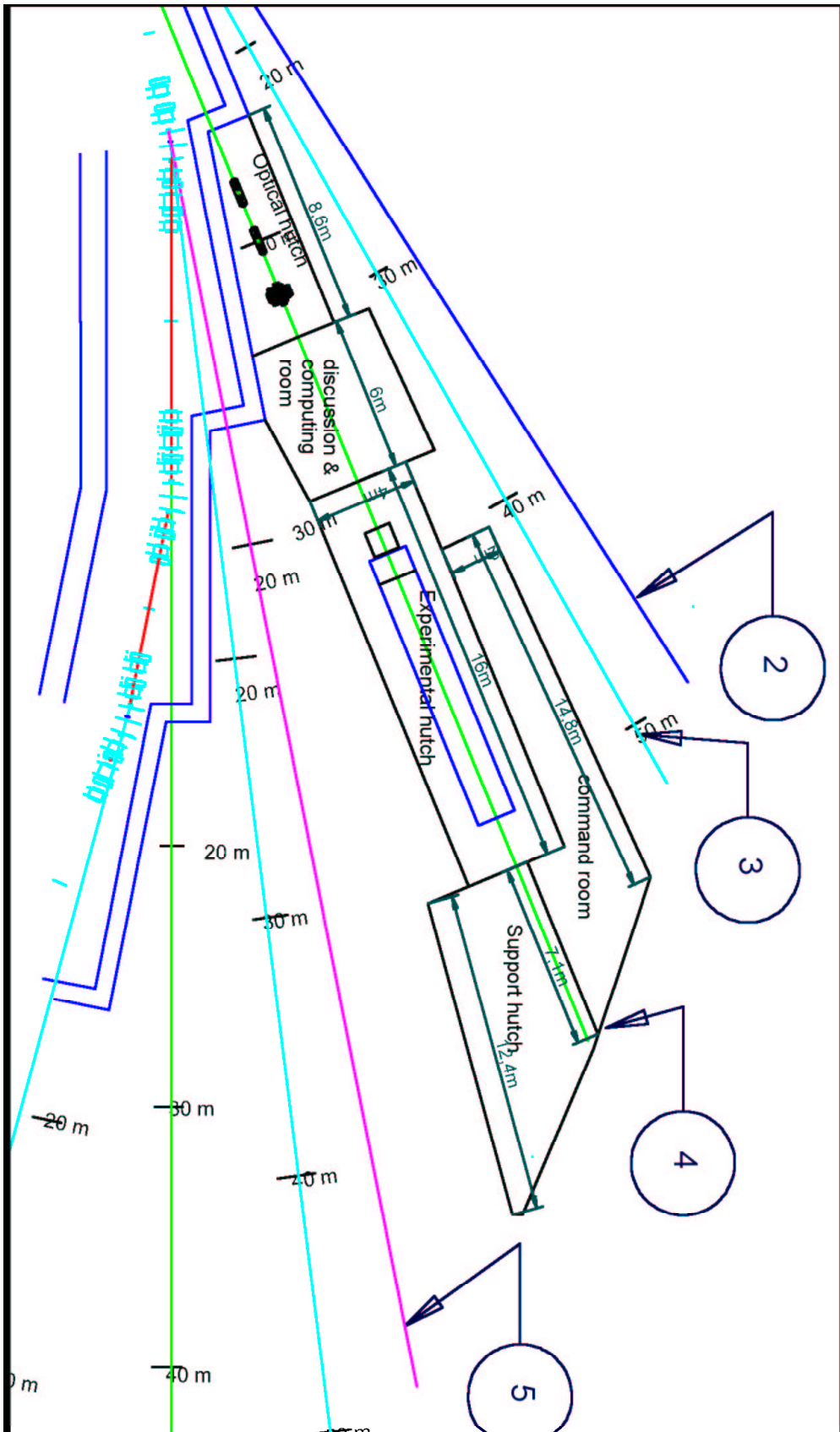


Figure 4 A possible implantation of the SAXS beam-line along a medium section beam path

## Appendix 1

# APS Small Angle Scattering Beamline

Thierry Moreno (Caminotec)  
Mourad IDIR (LSAI/LURE/SOLEIL)

### Summary

For the Small Angle Scattering Beamline, the source under consideration is a U26 undulator. The beamline is designed to be used from 5 to 15 keV.

For this beamline, the following general objectives should be met :

- high flux on the sample
- tunability between 5 and 15 keV
- resolution in energy  $\leq 10^{-4}$

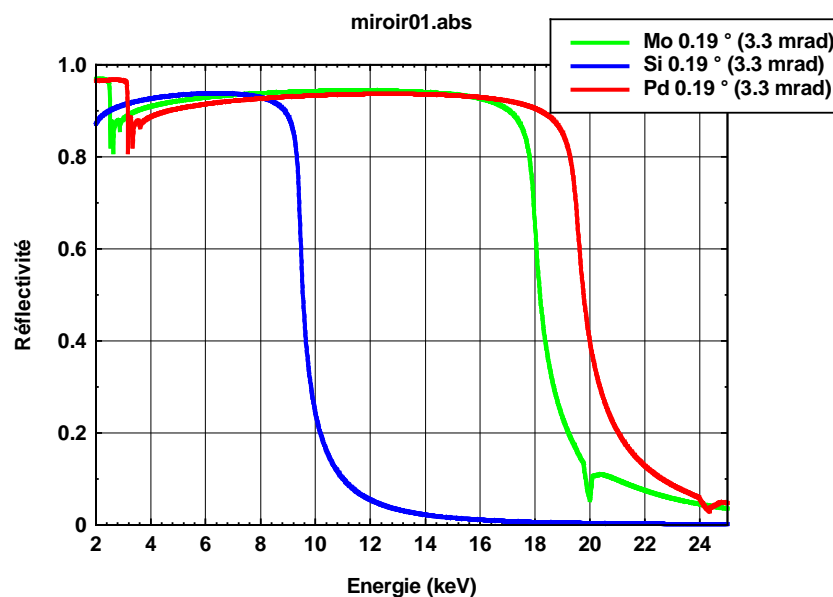
This report presents the expected result for the Small Angle Scattering Beamline on SOLEIL.

**Source : Undulator U26      Medium Section L=5.4 m 2 Modules (138 periods)**

	$\sigma_{ex}$ ( $\mu\text{m}$ )	$\sigma'_{ex}$ ( $\mu\text{rad}$ )	$\sigma_{ez}$ ( $\mu\text{m}$ )	$\sigma'_{ez}$ ( $\mu\text{rad}$ )
<b>Short Section (L=1.8 m)</b>	<b>388</b>	<b>14.5</b>	<b>8.08</b>	<b>4.61</b>
<b>Medium Section (L=5.4 m)</b>	<b>182</b>	<b>30.5</b>	<b>8.11</b>	<b>4.59</b>
<b>Long section</b>	<b>281</b>	<b>19.2</b>	<b>17.28</b>	<b>2.16</b>

**Table 1 : Electronic Source parameters**

For a Pd coated mirror working at  $0.2^\circ$  (3.5 mrad), the working energy range for a maximum reflectivity is from 5 to 17.5 keV. At the same angle, the working energy range for a Si mirror for maximum reflectivity is from 5 to 8 keV.



With this curve, it is clear that a mirror coated with two strips (Pd and Si) can be used to remove high order that may be reflected by the DCM. This mirror can be operated at an incident angle of  $0.2^\circ$  (3.5 mrad) and moved horizontally so that the critical angle can be adjusted to eliminate harmonics.

The location of all the optical components of the beamline is listed in table 2

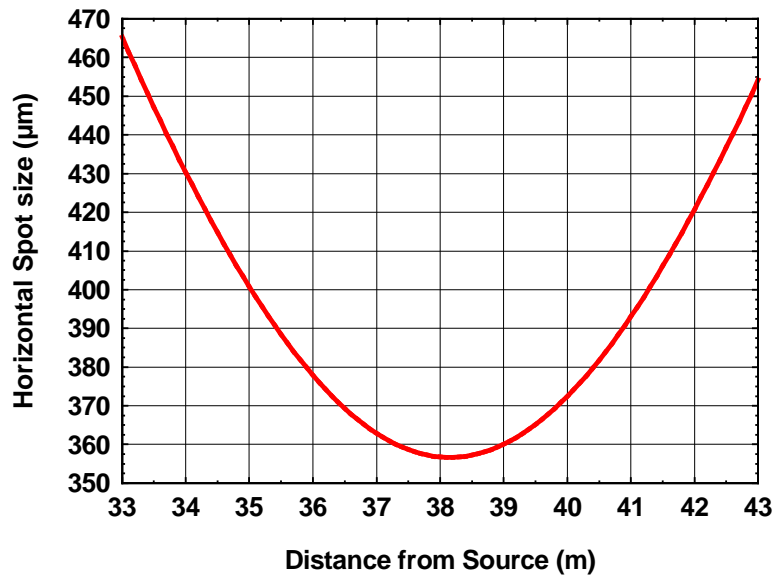
Optical component	Distance from the source (m)	Orientation (deg.)	size(mm)
Beam defining slit	15		1.5x0.5
Mirror 1 M1 Vertical focusing Pd 500 Å @ $0.2^\circ$	18 <i>p=18m</i> <i>q=18.1 m</i> <i>θ=0.2°</i> <i>R=5454 m</i>	0	50 x 250
Monochromator Si 111/Si 311	20	0-180	40 x 40
Mirror M2 Horizontal focusing Pd 500 Å @ $0.2^\circ$ Si @ $0.2^\circ$	22 <i>p=21 m</i> <i>q=30 m</i> <i>θ=0.2°</i> <i>R=5987 m</i>	90	50 x 500
“Sample”	38		

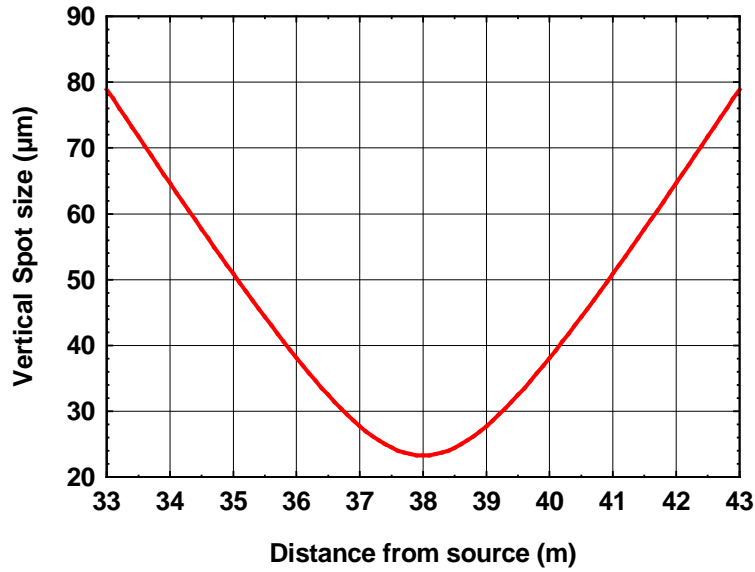
**Table : Position of the optical components.**

The second mirror (M2) will suppress the higher order harmonics of the energy selected while totally reflecting the useful energy.

On a medium section, a monochromatic spectral flux at 5 keV ( $K=1.8765$  harmonic  $n^5$ ) delivered by a Si(111) double-crystal monochromator of approximately  $1 \times 10^{14}$  photons/s/0.5 Amp will be focused on the sample in a spot size of  $\sim 352 \times 23$  (FWHM) with a divergence of  $\sim 75 \times 18$   $\mu$ rad in a bandwidth of 0.6 eV

### Estimation of the spot size versus the distance from the source





### Harmonic rejection

If the DCM is set at 5keV, around  $5 \times 10^9$  photons/s/0.5 Amp of the third harmonic will be focused on the sample using the Si part of the mirror (rejection factor : 1/ 20000).

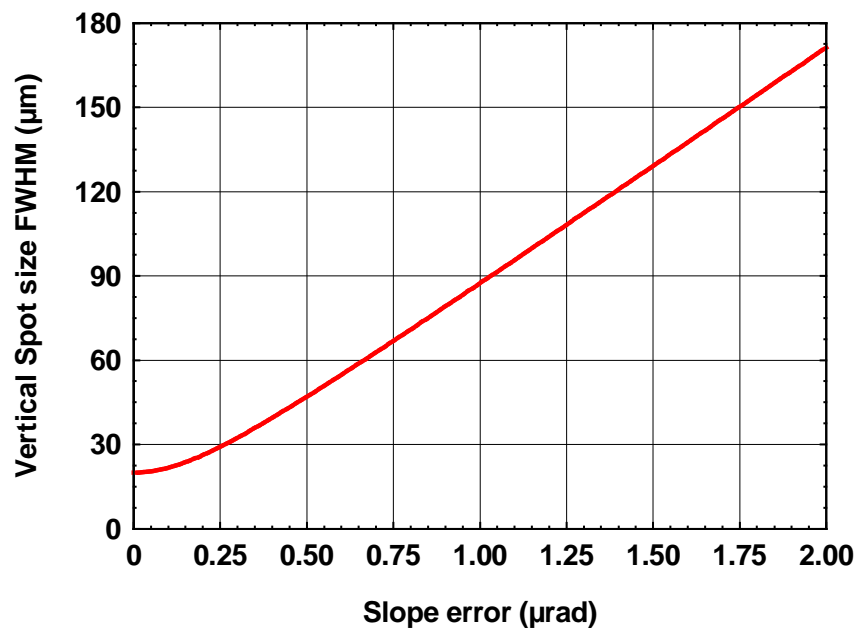
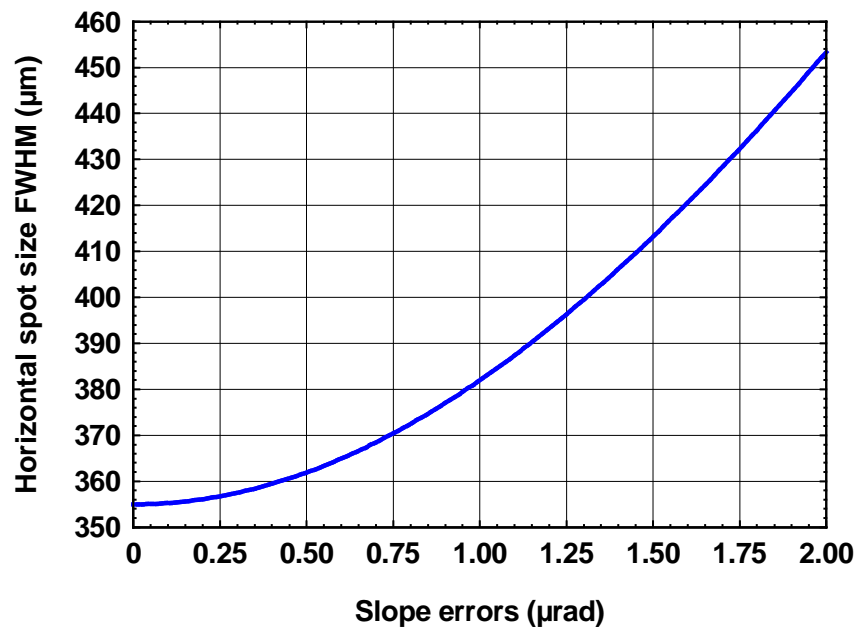
On a medium section, a monochromatic spectral flux at 15 keV ( $K=1.8765$  harmonic  $n^9$ ) delivered by a Si(311) double-crystal monochromator of approximately  $1 \times 10^{12}$  photons/s/0.5 Amp will be focused on the sample in a spot size of  $\sim 370 \times 21$  (FWHM) with a divergence of  $\sim 75 \times 20$   $\mu$ rad in a bandwidth of 1.1 eV

### Effect of the Slope errors on the spot size

We can estimate the effect of the focusing mirrors slope errors on the spot size with the following formula :

$$Spot = \sqrt{[(Slope(\mu rad)) \times (2 \times 2.35) \times (q(m))]^2 + \left(2.35 \sigma \frac{q}{p}\right)^2}$$

where Slope is the rms slope error of the mirror, q is the mirror-sample distance and  $\sigma$  is the source size.



## Support to the project

The following laboratories have sent letters of support to the project, expressing their interest and their plans to use the instrument for their future research. The indicated names are those of their respective correspondents, themselves representing one or several interested groups.

### Biology

Enrico Dainese  
Dipartimento di Strutture, Funzioni e Patologie Animali e Biotecnologie  
Universita degli Studi di Teramo  
P.zza A.Moro n. 5  
64100 Teramo, Italia

Michel Desmadril  
Directeur-adjoint de l'IBBMC  
Institut de Biochimie et de Biophysique Moléculaire et Cellulaire  
Faculté des Sciences d'Orsay  
Bâtiment 430  
91405 Orsay Cedex

Arnaud Ducruix  
Laboratoire de Cristallographie et RMN Biologiques  
UMR 8015 CNRS  
Faculté de Pharmacie  
4, Avenue de l'Observatoire  
75270 Paris cedex 06

Francoise Livolant  
Laboratoire de Physique des Solides  
Université Paris Sud  
Bat 510  
91405 Orsay Cedex

Jean-Luc Popot  
C.N.R.S. UPR 9052  
Institut de Biologie Physico-Chimique  
13, rue Pierre-et-Marie-Curie  
F-75005 PARIS

Véronique Receveur  
AFMB-CNRS  
31 Chemin Joseph Aiguier  
13402 Marseille cedex 20

Felix Rey  
CNRS UPR 9053  
Laboratoire de Génétique des Virus  
91198 Gif-Sur-Yvette Cedex

Jean-Pierre Samama  
C.N.R.S.-I.P.B.S.  
Groupe de cristallographie biologique

205 route de Narbonne  
31077 TOULOUSE Cedex

Annette Tardieu  
Equipe Interactions macromoléculaires  
Laboratoire de Minéralogie Cristallographie de Paris (LMCP)  
UMR 7590 CNRS - P6, P7.  
75005 Paris

Stéphane Veessler  
CRMC2-CNRS  
Campus de luminy case 913  
F-13288 Marseille Cedex 9

## **Soft Condensed Matter**

Marc AIRIAU  
Responsable Laboratoire de Caractérisation des Milieux Dispersés  
CRA/APC/CPH  
Rhodia Recherches  
52, rue de la Haie Coq, 93308 Aubervilliers.

Philippe Barois  
Directeur de Recherche  
Directeur du GDR 606  
Sous-Directeur du CRPP  
Avenue Albert Schweitzer,  
F-33600 PESSAC

Annie Brûlet  
LLB  
C.E. Saclay  
91191 Gif sur Yvette

Jean-Pierre Cotton  
Laboratoire Léon Brillouin  
CEA/Saclay  
91191 GIF/Yvette

Olivier Diat  
CEA Grenoble  
DSM/DRFMC/SI3M/PCI(polymères conducteurs ioniques)  
UMR SPAM 5819 (CEA-CNRS-Université J. Fourier)  
Bat. C5 P. 547  
17 av. des Martyrs  
38054 Grenoble Cedex 9

Patrick Davidson, Marianne Impéror  
Laboratoire de Physique des solides  
Bât 510  
Université Paris-Sud, 91405 Orsay

Michel OLLIVON  
UMR 8612 du CNRS  
Equipe Physico-Chimie des Systèmes Polyphasés  
Université Paris Sud  
5, rue J-B. Clément, 92296

Châtenay-Malabry

## **Metallurgy**

Pascal Andreatza  
Centre de Recherches sur la Matière Divisée  
CNRS - Université d'Orléans  
Orléans

Alain Dauger  
SPCTS - UMR CNRS n°6638  
ENSCI - 47 Av. Albert Thomas  
87065 Limoges

Evelyne Fargin, Thierry Cardinal  
Groupe des Matériaux pour l'optique  
Institut de Chimie de la Matière Condensée de Bordeaux  
Domaine universitaire  
33608 Pessac cedex

Thierry Gacoin  
Groupe de Chimie du Solide  
Laboratoire de Physique de la Matière Condensée  
Ecole Polytechnique  
91128 Palaiseau Cedex

Michael Gunnar Garnier  
Universität Basel  
Institut für Physik  
Klingelbergstrasse 82  
4056 Basel  
Switzerland

André Naudon  
Laboratoire de Métallurgie Physique  
UMR 6630 du CNRS  
UFR Sciences, bâtiment SP2MI ; Téléport 2,  
Bd Pierre et Marie Curie, BP 30179  
86962 Futuroscope-Chasseneuil Cedex

Bruno Palpant  
Laboratoire d'Optique des Solides  
Université Pierre et Marie Curie  
Case 80  
Tour 13, couloir 13/14, 4ème étage  
4, place Jussieu  
75252 Paris cedex 05

Frédéric Petroff  
Unité Mixte de Physique CNRS/THALES (CNRS-UMR137)  
Domaine de Corbeville  
91404 Orsay

Jean-Claude Pivin  
CSNSM-IN2P3  
Bâtiment 108  
Orsay Campus

91405 Orsay

Brigitte Prével  
DPM CNRS-UMR-5586  
Bat: L. Brillouin  
Université Claude Bernard Lyon 1  
43 Bd du 11 novembre 1918  
69622 Villeurbanne cédex

Christian Ricolleau  
Laboratoire de Minéralogie-Cristallographie de Paris (LMCP)  
Université Paris 7 - Denis Diderot / CNRS UMR 7590  
75005 Paris

Colette Servant  
Laboratoire de Métallurgie Physique  
Université Paris-Sud  
91405 Orsay

Rosalía Serna  
Instituto de Optica, CSIC, Serrano 121  
28006 Madrid, Spain

## **Others**

Fabien Thomas, Assistant Director of LEM, and several groups in the lab.  
Laboratoire Environnement et Minéralurgie (UMR 7569 CNRS-INPL)  
15, Avenue du Charmois  
BP 40  
F-54501 Vandoeuvre Les Nancy Cedex

## Bibliographic references

- [1] Svergun, D. I. & Nierhaus, K. H. (2000). A map of protein-rRNA distribution in the 70 S Escherichia coli ribosome. *J. Biol. Chem.* **275**(19), 14432-9.
- [2] Zhao, J., Hoye, E., Boylan, S., Walsh, D. A. & Trewella, J. (1998). Quaternary structures of a catalytic subunit-regulatory subunit dimeric complex and the holoenzyme of the cAMP-dependent protein kinase by neutron contrast variation. *J. Biol. Chem.* **273**(46), 30448-59.
- [3] Fetler, L., Tauc, P., Hervé, G., Moody, M. F. & Vachette, P. (1995). X-ray scattering titration of the quaternary structure transition of aspartate transcarbamylase with a bisubstrate analogue: influence of nucleotide effectors. *J. Mol. Biol.* **251**(2), 243-55.
- [4] Egea, P. F., Rochel, N., Birck, C., Vachette, P., Timmins, P. A. & Moras, D. (2001). Effects of Ligand Binding on the Association Properties and Conformation in Solution of Retinoic Acid Receptors RXR and RAR. *J. Mol. Biol.* **307**, 557-576.
- [5] Grossmann, J. G., Crawley, J. B., Strange, R. W., Patel, K. J., Murphy, L. M., Neu, M., Evans, R. W. & Hasnain, S. S. (1998). The nature of ligand-induced conformational change in transferrin in solution. An investigation using X-ray scattering, XAFS and site-directed mutants. *J. Mol. Biol.* **279**(2), 461-72.
- [6] Koenig, S., Svergun, D. I., Volkov, V. V., Feigin, L. A. & Koch, M. H. J. (1998). Small-angle X-ray solution-scattering studies on ligand-induced subunit interactions of the thiamine diphosphate dependent enzyme pyruvate decarboxylase from different organisms. *Biochemistry* **37**(15), 5329-34.
- [7] Sokolova, A., Malfois, M., Caldentey, J., Svergun, D. I., Koch, M. H. J., Bamford, D. H. & Tuma, R. (2001). Solution structure of bacteriophage PRD1 vertex complex. *J. Biol. Chem.* **27**, 27.
- [8] Lata, R., Conway, J. F., Cheng, N., Duda, R. L., Hendrix, R. W., Wikoff, W. R., Johnson, J. E., Tsuruta, H. & Steven, A. C. (2000). Maturation dynamics of a viral capsid: visualization of transitional intermediate states. *Cell* **100**(2), 253-63.
- [9] Glatter, O. (1977). A new method for the evaluation of small-angle scattering data. *J. Appl. Crystallogr.* **10**, 415-421.
- [10] Chacon, P., Diaz, J. F., Moran, F. & Andreu, J. M. (2000). Reconstruction of protein form with X-ray solution scattering and a genetic algorithm. *J. Mol. Biol.* **299**, 1289-1302.
- [11] Konarev, P. V., Petoukhov, M. V. & Svergun, D. I. (2001). MASSHA - a graphic system for rigid body modelling of macromolecular complexes against solution scattering data. *J. Appl. Crystallogr.* **34**, 527-532.
- [12] Svergun, D. I., Barberato, C. & Koch, M. H. J. (1995). CRY SOL - a program to evaluate X-ray solution scattering of biological macromolecules from atomic coordinates. *J. Appl. Crystallogr.* **28**, 768-773.
- [13] Svergun, D. I. (1999). Restoring low resolution structure of biological macromolecules from solution scattering using simulated annealing. *Biophys. J.* **76**, 2879-2886.
- [14] Svergun, D. I., Petoukhov, M. V. & Koch, M. H. J. (2001). Determination of domain structure of proteins from X-ray solution scattering. *Biophys. J.* **80**, 2946-2953.
- [15] Berman, H. M., Westbrook, J., Feng, Z., Gilliland, G., Bhat, T. N., Weissig, H., Shindyalov, I. N. & Bourne, P. E. (2000). The Protein Data Bank. *Nucleic Acids Res.* **28**(1), 235-42.

- [16] Svergun, D. I., Barberato, C., Koch, M. H. J., Fetler, L. & Vachette, P. (1997). Large differences are observed between the crystal and solution quaternary structures of allosteric aspartate transcarbamylase in the R state. *Proteins* **27**(1), 110-117.
- [17] Svergun, D. I., Petoukhov, M. V., Koch, M. H. J. & Koenig, S. (2000). Crystal versus solution structures of thiamine diphosphate-dependent enzymes. *J. Biol. Chem.* **275**(1), 297-302.
- [18] Nakasako, M., Fujisawa, T., Adachi, S., Kudo, T. & Higuchi, S. (2001). Large-scale domain movements and hydration structure changes in the active-site cleft of unligated glutamate dehydrogenase from *Thermococcus profundus* studied by cryogenic X-ray crystal structure analysis and small-angle X-ray scattering. *Biochemistry* **40**(10), 3069-79.
- [19] Yuzawa, S., Yokochi, M., Hatanaka, H., Ogura, K., Kataoka, M., Miura, K., Mandiyan, V., Schlessinger, J. & Inagaki, F. (2001). Solution Structure of Grb2 Reveals Extensive Flexibility Necessary for Target Recognition. *J. Mol. Biol.* **306**, 527-537.
- [20] Hamiaux, C., Pérez, J., Prangé, T., Veesler, S., Riès-Kautt, M. & Vachette, P. (2000). The BPTI decamer observed in acidic pH crystal forms pre-exists as a stable species in solution. *J. Mol. Biol.* **297**, 697-712.
- [21] Svergun, D. I., Aldag, I., Sieck, T., Altendorf, K., Koch, M. H. J., Kane, D. J., Kozin, M. B. & Grueber, G. (1998). A model of the quaternary structure of the *Escherichia coli* F1 ATPase from X-ray solution scattering and evidence for structural changes in the delta subunit during ATP hydrolysis. *Biophys. J.* **75**(5), 2212-9.
- [22] Plaxco, K. W., Millett, I. S., Segel, D. J., Doniach, S. & Baker, D. (1999). Chain collapse can occur concomitantly with the rate-limiting step in protein folding. *Nat. Struct. Biol.* **6**(6), 554-6.
- [23] Segel, D. J., Bachmann, A., Hofrichter, J., Hodgson, K. O., Doniach, S. & Kiefhaber, T. (1999). Characterization of transient intermediates in lysozyme folding with time-resolved small-angle X-ray scattering. *J. Mol. Biol.* **288**(3), 489-99.
- [24] Russell, R., Millett, I. S., Doniach, S. & Herschlag, D. (2000). Small angle X-ray scattering reveals a compact intermediate in RNA folding. *Nat. Struct. Biol.* **7**(5), 367-70.
- [25] Perez, J., Vachette, P., Russo, D., Desmadril, M. & Durand, D. (2001). Heat-induced unfolding of neocarzinostatin, a small all-beta protein investigated by small-angle X-ray scattering. *J Mol Biol* **308**(4), 721-43.
- [26] Akiyama, S., Takahashi, S., Kimura, T., Ishimori, K., Morishima, I., Nishikawa, Y. & Fujisawa, T. (2002). Conformational landscape of cytochrome c folding studied by microsecond-resolved small-angle x-ray scattering. *Proc Natl Acad Sci U S A* **2**, 2.
- [27] Tardieu, A., Bonneté, F., Finet, S. & Vivarès, D. (2002). Towards the control of biomolecular crystallization. In *Macromolecular Crystallography, Part C* (Carter, C. W. J. & Sweet, R. M., eds.). Academic Press.
- [28] Tsuruta, H., Vachette, P., Sano, T., Moody, M. F., Amemiya, Y., Wakabayashi, K. & Kihara, H. (1994). Kinetics of the quaternary structure change of aspartate transcarbamylase triggered by succinate, a competitive inhibitor. *Biochemistry* **33**(33), 10007-12.
- [29] Tsuruta, H., Reddy, V. S., Wikoff, W. R. & Johnson, J. E. (1998). Imaging RNA and dynamic protein segments with low-resolution virus crystallography: experimental design, data processing and implications of electron density maps. *J. Mol. Biol.* **284**(5), 1439-52.
- [30] See, for example, *ARAGO 27, Nanomatériaux, OFTA, Paris*.(2001).

- [31] Simon, J.-P. & Lyon, O. (1987). *Phys. Rev.* **B35**, 5164-5174.
- [32] Lyon, O., Guillon, I. & Servant, C. (2001). *J. Appl. Crystallogr.* **34**, 484-492.
- [33] Gonella, F., Cattaruzza, E., Battaglin, G., D'Acapito, F., Sada, C., Mazzoldi, P., Maurizio, C., Mattei, G., Martorana, A., Longo, A. & Zontone, F. (2001). *J. Non-Cryst. Solids* **280**, 241-248.
- [34] Thomann, A.-L., Rozenbaum, J.-P., Brault, P., Andrezza-Vignole, C. & Andrezza, P. (2000). *Appl. Surf. Sci.* **158**, 172-183.
- [35] neau, D., Briatico, J., Petroff, F., Cabioch, T. & Naudon, A. (2000). *J. Appl. Phys.* **87**, 3432-3443.
- [36] Babonneau, D., Petroff, F., Maurice, J.-L., Fettar, F., Vaurès, A. & Naudon, A. (2000). *Appl. Phys. Lett.* **76**, 2892-2894.
- [37] Levine, J. R., Cohen, J. B., Chung, Y. W. & Georgopoulos, P. (1989). *J. Appl. Crystallogr.* **22**, 528-532.
- [38] Babonneau, D., Naudon, A., Cabioch, T. & Lyon, O. (2000). *J. Appl. Crystallogr.* **33**, 437-441.
- [39] Rauscher, M., Paniago, R., Metzger, H., Kovats, Z., Domke, J., Peisl, J., Pfannes, H.-D., Schulze, J. & Eisele, I. (1999). *J. Appl. Phys.* **86**, 6763-6769.
- [40] Stangl, J., Holý, V., Roch, T., Daniel, A., Bauer, G., Zhu, J., Brunner, K. & Abstreiter, G. (2000). *Phys. Rev.* **B62**, 7229-7236.
- [41] Van den Bossche, G., Sobry, R., Clacens, J. M. & Gabelica, Z. (1997). Characterization of hexagonal and lamellar mesoporous silicas, alumino- and gallosilicates by small-angle X-ray scattering. *J. Appl. Cryst.* **30**, 1065.
- [42] De Moor, P. P. E. A., Beelen, T. P. M., Komanchek, B. U., Diat, O. & Van Santen, R. A. (1997). In situ investigation of Si- TPA- MFI crystallization using (ultra-)small- and wide-angle X-ray scattering techniques. *J. Phys. Chem.B* **101**, 11077.
- [43] Carion-Taravella, B., Lesieur, S., Ollivon, M. & Chopineau, J. (1998). DPPC vesicles formation by amyloglucosidase reaction on mixed micelles. *J. Am. Chem. Soc.* **41**, 10588.
- [44] Constantin, D., Oswald, P., Imperor-Clerc, M., Davidson, P. & Sotta, P. (2001). Connectivity of the hexagonal, cubic, and isotropic phases of the C12EO6/ H2O lyotropic mixture investigated by tracer diffusion and X-ray scattering. *J. Phys. Chem. B* **105**, 668.
- [45] Dhez, O., Koning, S., Nallet, F., Roux, D. & Diat, O. (2000). Lamellar to nematic phase transition in a lipid-surfactant mixture. *Eur. Phys. J. E* **3**, 377.
- [46] Dubois, M., Zemb, T., Fuller, N., Rand, R. P. & Parsegian, V. A. (1998). Equation of state of a charged bilayer system : measure of the entropy of the lamellar-lamellar transition in DDABr. *J. Chem. Phys.* **108**(18), 7855-7869.
- [47] Dubois, M. & Zemb, T. (1998). Mesure des forces moléculaires entre bicouches par diffusion de rayons-X à pression osmotique contrôlée. *J. Phys. IV France* **8**, 55-62.
- [48] Dubois, M., Demé, B., Gulik-Krzywicki, T., Dedieu, J.-C., Vautrin, C., Désert, S., Perez, E. & Zemb, T. (2001). Self-assembly of regular hollow icosahedra in salt-free catanionic solutions. *Nature* **411**, 672.
- [49] Ollivon, M., Paternostre, M., Lesieur, S. & Grabielle-Madelmont, C. (2000). Vesicle reconstitution from lipid-detergent mixed micelles. *Biochim. Biophys. Acta* **1508**(Special issue of BBA Biomembranes, guest editors F. Goni and A. Alonso), 34.
- [50] Rappolt, M., Pabst, G., Rapp, G., Kriechbaum, M., Amenitsch, H., Krenn, C., Bernstorff, S. & Laggner, P. (2000). New evidence for gel-liquid crystalline phase coexistence in the ripple phase of phosphatidylcholines. *European Biophysical Journal* **29**, 125.

- [51] Ricoult, F., Dubois, M., Zemb, T., Vandais, A., Plusquellec, D., Rico-Lattes, I. & Diat, O. (1998). An efficient method to determine isothermal ternary phase diagrams using SAXS. *J. Phys. Chem. B* **102**, 2769.
- [52] Warriner, H. E., Idziak, S. H. J., Slack, N. L., Davidson, P. & Safinya, C. R. (1996). Lamellar biogels: fluid-membranebased hydrogels containing polymer-lipids. *Science* **271**, 969.
- [53] Thurn-Albrecht, T., Meier, G., Muller-Buschbaum, P., Patkowski, A., Steffen, W., Grubel, G., Abernathy, D. L., Diat, O., Winter, M., Koch, M. & Reetz, M. T. (1999). Structure and dynamics of surfactant-stabilized aggregates of palladium nanoparticles under dilute and semidilute conditions: static and dynamic X-ray scattering. *Phys. Rev. E* **59 (1-B)**, 642.
- [54] Slack, N. L., Davidson, P., Chibbaro, M. A., Jeppesen, C., Eiselt, P., Warriner, H. E., Schmidt, H. W., Pincus, P. & Safinya, C. (2001). The bridging conformations of double-end anchored polymer-surfactants destabilize a hydrogel of lipid membranes. *J. Chem. Phys.* **115**, 6252.
- [55] Andrieux, K., Forte, L., Keller, G., Grabielle-Madelmont, C., Lesieur, S., Paternostre, M., Ollivon, M., Bourgaux, C. & Lesieur, P. (1998). Study of DPPC/TC/water phase diagram by coupling of synchrotron SAXS and DSC: I. Equilibration kinetics. *Prog. Colloid Polym. Sci.* **110**, 280.
- [56] Angelov, B., Ollivon, M. & Angelova, A. (1999). X-ray diffraction study of the effect of the detergent octylglucoside on the structures of lamellar and nonlamellar lipid/water phases for membrane protein reconstitution. *Langmuir* **15**, 8225.
- [57] Forte, L., Andrieux, K., Keller, G., Grabielle-Madelmont, C., Lesieur, S., Paternostre, M., Ollivon, M., Bourgaux, C. & Lesieur, P. (1998). Sodium taurocholate-induced lamellar-micellar phase transitions of DPPC-determined by DSC and X-ray diffraction. *J. Therm. Anal. Calorim.* **51(3)**, 773.
- [58] Radler, J. O., Koltover, I., Salditt, T. & Safinya, C. R. (1997). Structure of DNA-cationic liposome complexes: DNA intercalation in multilamellar membranes in distinct interhelical packing regimes. *Science* **275**, 810.
- [59] Koltover, I., Salditt, T., Radler, J. O. & Safinya, C. R. (1998). An inverted hexagonal phase of DNA-cationic liposome complexes: structure to gene release mechanism correlations. *Science* **281**, 78.
- [60] Artzner, F., Zantl, R., Rapp, G. & Radler, J. O. (1998). Observation of a rectangular columnar phase in condensed lamellar cationic lipid-DNA complexes. *Phys. Rev. Lett.* **81(22)**, 5015.
- [61] Grabielle-Madelmont, C., Hochapfel, A. & Ollivon, M. (1999). Antibiotic-Phospholipid interactions as studied by DSC and X-ray diffraction. *J. Phys. Chem. B* **103**, 4534.
- [62] Lopez, C., Lesieur, P., Bourgaux, C. & Ollivon, M. (2000). Thermal and structural behaviour of milk fat: 1 Unstable species of cream. *J. Colloid Interf. Sci.* **299**, 62.
- [63] Lopez, C., Lesieur, P., Bourgaux, C., Keller, G. & Ollivon, M. (2001). Thermal and structural behavior of milk fat: 2. Crystalline forms obtained by slow cooling of cream. *J. Colloid Interf. Sci.* **240**, 150.
- [64] Imperor-Clerc, M., Davidson, P. & Davidson, A. (2000). Existence of a microporous corona around the mesopores of silica-based SBA-15 materials templated by triblock copolymers. *J. Am. Chem.Soc.* **122**, 11925.
- [65] Babonneau, F., Leite, L., Fontlupt, S., Ribot, F., Bergogne, L. & Roux, C. (1998). Synthesis and structural characterization of organically-modified microporous silicates. *Mater. Res. Soc. Symp. Proc.* **519**, 363.

- [66] Boissiere, C., Larbot, A., Bourgaux, C., Prouzet, E. & Bunton, C. A. (2001). A study of the assembly mechanism of the mesoporous MSU-X silica two-step synthesis. *Chem. Mater.* **13**, 3580.
- [67] Davidson, P., Bourgaux, C., Schouffet, L., Sergot, P., Williams, C. & Livage, J. (1995). A structural study of the lyotropic nematic phase of vanadium pentoxide gels. *J. de Physique II* **5**, 1577.
- [68] Pelletier, O., Bourgaux, C., Diat, O., Davidson, P. & Livage, J. (1999). A biaxial nematic gel phase in aqueous vanadium pentoxide suspensions. *Eur. Phys. Journal B* **12**, 541.
- [69] Pelletier, O., Bourgaux, C., Diat, O., Davidson, P. & Livage, J. (2000). A small angle X-ray scattering study of the isotropic and nematic phases of V<sub>2</sub>O<sub>5</sub> suspensions. *Eur. Phys. Journal E* **2**, 191.
- [70] Gabriel, J. C., Camerel, F., Lemaire, B. J., Desvaux, H., Davidson, P. & Batail, P. (2001). Swollen liquid-crystalline lamellar phase based on extended solid-like sheets. *Nature* **413**, 504.
- [71] Megens, M., van Kats, C. M., Bosecke, P. & Vos, W. L. (1997). Synchrotron small-angle X-ray scattering of colloids and photonic colloidal crystals. *Journal of Applied Crystallography* **30**, 637.
- [72] Beysens, D. & Narayanan, T. (1999). Wetting-induced aggregation of colloids. *Journal of Statistical Physics* **95**, 997.
- [73] Brown, A. B. D., Ferrero, C., Narayanan, T. & Rennie, A. R. (1999). Phase separation and structure in a concentrated colloidal dispersion of uniform plates. *European Physical Journal B* **11**, 481.
- [74] Ramzi, M., Rochas, C. & Guenet, J. M. (1998). Structure- properties relation for agarose thermoreversible gels in binary solvents. *Macromolecules* **31**, 6106.
- [75] Djurado, D., Curtet, J. P., Legrand, J. F., Bee, M., Michot, C. & Armand, M. (1997). Structure and microstructure of mixed ionic electronic conducting alternate copolymers. *Synt. met.* **84**, 989.
- [76] Djurado, D., Bee, M., Curtet, J. P., Legrand, J. F., Bourgaux, C., Michot, C. & Armand, M. (1998). Structure evolution of (BDTA(PEO)<sub>x</sub>)<sub>n</sub> alternate copolymers when mixed with a lithium salt. *Journal de Chimie Physique* **95**, 1539.
- [77] Paternostre, L., Damman, P. & Dosiere, M. (1997). Time-resolved SAXS study of the crystallization and melting of Poly(ethylene oxide) molecular complexes. *Macromol.* **30**, 3946.
- [78] Sobry, R., Van den Bossche, G., Fontaine, F., Gohy, J. F. & Jerome, R. (1997). Small angle X-ray scattering and small angle neutron scattering study of liquid crystalline halato(semi)telechelic polymers. *J. Appl. Cryst.* **30**, 1075.
- [79] Gohy, J. F., Jerome, R., van den Bossche, G. & Sobry, R. (1998). Supramolecular organization of model liquid crystalline ionomers. *Macromol. Chem. Phys.* **199**, 1791.
- [80] Blundell, D. J., Mahendrasingam, A., Martin, C., Fuller, W., MCKerron, D. H., Harvie, J. L., Oldman, R. J. & Riekel, C. (2000). Orientation prior to crystallisation during drawing of poly(ethylene terephthalate). *Polymer* **41**, 7793.
- [81] Geissler, E., Hecht, A. M., Rochas, C., Bley, F., Livet, F. & Sutton, M. (2000). Aging in a filled polymer: coherent small angle X-ray and light scattering. *Physical Review E* **62**, 8308.
- [82] Heidelbach, F., Riekel, C. & Wenk, H. R. (1999). Quantitative texture analysis of small domains with synchrotron radiation X-ray. *Journal of Applied Crystallography* **32**, 841.

- [83] Lorenzen, M. (1999). In-situ X-ray structural and morphological studies of synthetic polymers under pressure. *Recent Research Developments in Macromolecules Research* **4**, 95.
- [84] Mahendrasingam A., Blundell D.J., Martin C., Fuller W., MCKerron D.H., Harvie J.L., Oldman R.J. & Riekkel C. (2000). Influence of temperature and chain orientation on the crystallization of poly(ethylene terephthalate) during fast drawing. *Polymer* **41**, 7803.
- [85] Muller, M., Riekkel, C., Vuong, R. & Chanzy, H. (2000). Skin/core micro-structure in viscose rayon fibres analysed by X-ray microbeam and electron diffraction mapping. *Polymer* **41**, 2627.
- [86] Rastogi, S., Goossens, J. G. P. & Lemstra, P. J. (1998). An in situ SAXS/WAXS/Raman spectroscopy study on the phase behavior of syndiotactic polystyrene (sPS)/solvent systems: Compound formation and solvent (Dis)ordering. *Macromolecules* **31**, 2983.
- [87] Hamley, I. W., Pople, J. A., Booth, C., Dericci, L., Imperor-Clerc, M. & Davidson, P. (1998). Shear- induced orientation of the body-centered cubic phase in a diblock copolymer gel. *Phys. Rev. E* **58**, 7620.
- [88] Leyh, B., Creutz, S., Gaspard, J. P., Bourgaux, C. & Jerome, R. (1998). Shear-induced order in aqueous micellar solutions of amphiphilic poly(tert-butylstyrene)-b-poly(Na methacrylate) diblocks. *Macromol.* **31**, 9258.
- [89] Diat, O., Berret, J. F. & Porte, G. (1996). Shear induced ordering in micellar cubic phases. *Phys. Rev. B condensed matter* **54**(21), 14869.
- [90] Koltover, I., Idziak, S. H. J., Davidson, P., Li, Y., Safinya, C. R., Ruths, M., Steinberg, S. & Israelachvili, J. N. (1996). Alignment of complex fluids under confinement and flow. *J. de Physique II* **6**, 893.
- [91] Imperor-Clerc, M. & Davidson, P. (1999). An X-ray scattering study of flow-aligned samples of a lyotropic liquid- crystalline hexagonal phase. *European Physical Journal B* **9**, 93.
- [92] Mahjoub, H., Bourgaux, C., Sergot, P. & Kleman, M. (1998). Evidence of a sponge-to-lamellar phase transition under shear by X-ray scattering experiments in a Couette cell. *Phys. Rev. Lett.* **81**, 2076.
- [93] Meyer, C., Asnacios, S., Bourgaux, C. & Kleman, M. (1999). Effects of shear on a lyotropic lamellar phase. *Mol. Cryst. and Liq. Cryst. Science and technology Section A* **332**, 3041.
- [94] Meyer, C., Asnacios, S., Bourgaux, C. & Kleman, M. (2000). Rheology of lyotropic and thermotropic lamellar phases. *Rheologica Acta* **39**(3), 223.
- [95] Dhez, O., Nallet, F. & Diat, O. (2001). Influence of screw dislocations on the orientation of a sheared lamellar phase. *Europhys. Lett.* **55**(6), 821.
- [96] Viletti, M., Borsali, R., Diat, O., Soldi, V. & Fukada, K. (2000). SAXS from polyelectrolyte solutions under shear: Xanthan and Na-Hyaluronate examples. *Macromol.* **33**, 9418.
- [97] Tsuruta, H., Brennan, S., Rek, Z. U., Irving, T. C., Tompkins, W. H. & Hodgson, K. O. (1998). A Wide-Bandpass Multilayer Monochromator for Biological Small-Angle Scattering and Fiber Diffraction Studies. *J. Appl. Crystallogr.* **31**, 672-682.
- [98] Riekkel, C. (2000). New avenues in X-ray microbeam experiments. *Reports on Progress in Physics* **63**, 233.
- [99] Riekkel, C., Burghammer, M. & Muller, M. (2000). Microbeam small-angle scattering experiments and their combination with microdiffraction. *Journal of Applied crystallography* **33**, 421.